

Diss. ETH No. 9584

Prof. Dr. Fritz K. Kneubühl  
Institut für Quantenelektronik  
Physik-Departement  
Eidgenössische Technische Hochschule  
HPF, Hönggerberg  
CH-8093 Zürich, Schweiz

*F. Kneubühl*  
17.12.91

**DEVELOPMENT AND OPTIMIZATION  
OF  
OFID-10  $\mu\text{m}$  CO<sub>2</sub>  
LASER SYSTEMS**

A dissertation submitted to the  
**SWISS FEDERAL INSTITUTE OF TECHNOLOGY, ZUERICH**  
for the degree of  
**Doctor of Technical Sciences**

presented by  
**ARMIN WALTER KÄLIN**  
Dipl. El. Ing. ETH  
born May 24, 1958  
citizen of Einsiedeln/Schwyz

accepted on the recommendation of  
**Prof. Dr. F. K. Kneubühl**  
**Prof. Dr.-Ing. W. S. Zaengl**

1991

*To Marianne, Lucy, Lucas*

# DEVELOPMENT AND OPTIMIZATION OF OFID-10 $\mu\text{m}$ CO<sub>2</sub> LASER SYSTEMS

---

## Table of Contents

---

Zusammenfassung .....	1
Summary .....	3
<b>1 Introduction .....</b>	<b>5</b>
1.1 Survey .....	5
1.2 Transversely Excited CO <sub>2</sub> Lasers .....	6
1.3 Short-Pulse CO <sub>2</sub> Lasers .....	9
<b>2 OFID-System.....</b>	<b>11</b>
2.1 Concept .....	11
2.2 Principle of Optical Free Induction Decay .....	12
2.3 Linear System Analysis .....	15
<b>3 Single-Longitudinal-Mode Hybrid 10 <math>\mu\text{m}</math> CO<sub>2</sub> Laser.....</b>	<b>19</b>
3.1 Single-Longitudinal-Mode Operation .....	19
3.2 Hybrid-CO <sub>2</sub> -Laser-System I.....	23
3.3 Hybrid-CO <sub>2</sub> -Laser-System II .....	25
3.3.1 System Design .....	25
3.3.2 Uniform-Field Electrodes Design.....	25
3.3.3 Dielectric Corona Preionization.....	28
3.3.4 Optical Resonator.....	33
3.3.5 Performance .....	34

<b>4</b>	<b>The Plasma Shutter .....</b>	<b>36</b>
4.1	Principle of Operation .....	36
4.2	Design of the Plasma Shutter .....	38
4.3	Targets for Optical Triggering .....	39
4.4	Electrical Triggering by a Laser Triggered Spark Gap .....	42
<b>5</b>	<b>The Hot CO<sub>2</sub>-Cell .....</b>	<b>48</b>
5.1	Spectral Filters in Short-Pulse Systems .....	48
5.2	Previous Designs .....	48
5.3	Present Design .....	50
<b>6</b>	<b>OFID-Pulse Characteristics .....</b>	<b>53</b>
6.1	Theoretical Pulse Shapes .....	53
6.2	Direct Pulse Measurements .....	57
6.3	Autocorrelation Pulse Measurements .....	58
6.4	Multiple Breakdown Phenomena .....	63
<b>7</b>	<b>Conclusion .....</b>	<b>65</b>
<b>8</b>	<b>References .....</b>	<b>66</b>
	Acknowledgement .....	82
	Curriculum Vitae .....	83

## Zusammenfassung

*Eine weitverbreitete Methode um kurze Laserpulse zu erzeugen ist die Mode-locking Technik. Eine alternative Möglichkeit, welche im 10  $\mu\text{m}$  Wellenlängenbereich kürzere Pulse als diejenigen der Mode-locking Technik produziert, ist die Erzeugung von Seitenbandfrequenzen durch schnelle Amplitudenmodulation und durch anschliessendes Ausfiltern der Grundfrequenz. Die Amplitudenmodulation geschieht durch ein optisches Gasdurchbruchplasma, welches den einfallenden 100 ns Puls in etwa 10 ps abschneidet. Als spektrales Filter ergibt resonant absorbierendes, heisses  $\text{CO}_2$  Gas ein ausgezeichnetes Puls/Untergrund-Kontrast Verhältnis. Im heissen  $\text{CO}_2$  Gas wird der kurze Puls durch den optischen freien Induktionszerfall erzeugt, einem physikalischen Prozess analog dem freien Induktionszerfall bei nuklearer magnetischer Resonanz. Der optische freie Induktionszerfall wurde erstmals vor etwa fünfzehn Jahren benutzt um kurze  $\text{CO}_2$  Laser Pulse zu erzeugen. Bis jetzt jedoch gab es wenige Anwendungen. Das Hauptproblem lag bei der Reproduzierbarkeit des schnellen Abschneidens eines TEA-Laser Pulses durch einen zuverlässigen, ausreichend schnellen optischen Schalter. Ein weiteres Problem ist das Fehlen von kommerziell erhältlichen Hochleistungs-TEA-Lasern, die auf einer einzigen Frequenz oszillieren.*

*Die vorliegende Arbeit beschreibt zwei auf dem optischen freien Induktionszerfall basierende Kurzpuls-Lasersysteme, die sich hauptsächlich im Pump-Laser und in der Spitzenleistung der kurzen Pulse unterscheiden. Unsere verbesserten Plasma-Schalter als optische Schalter arbeiten mit variablen Gasdrücken und werden durch ein lasererzeugtes Oberflächenplasma oder durch eine elektrische Hochspannungsentladung gesteuert. Für das Oberflächenplasma haben wir neue Target-Materialien gefunden. Die elektrische Entladung wird durch den TEA-Laserpuls über eine neuentwickelte lasergesteuerte Funkenstrecke ausgelöst. Ferner wurde auch ein TEA- $\text{CO}_2$ -Laser mit einer neuartigen Oberflächen-Korona-Vorionisation entwickelt. Dieser bildet zusammen mit einem kontinuierlich*

*angeregten Niederdruckteil einen Hochleistungs-Hybrid-CO<sub>2</sub>-Laser, welcher die benötigten Einfrequenzpulse liefert. Eine elektronische Steuerung ergänzt die Systeme zu zuverlässigen Forschungswerkzeugen, die der Forscher durch ein paar Knopfdrücke bedienen kann. Beide Systeme erzeugen kurze 10 μm Pulse, mit einer Dauer von minimal 30 ps. Da eine direkte, zeitaufgelöste Messung der Intensität der kurzen Pulse nicht möglich ist, werden numerische Berechnungen benötigt, um den Einfluss verschiedener Parameter auf Pulsform und -dauer abzuschätzen. Schliesslich haben wir durch optische Autokorrelationsmessungen mit Hilfe der Erzeugung der zweiten Harmonischen bewiesen, dass die erwarteten Pulsdauern erreicht werden.*

## Summary

*A common method to generate short laser pulses is the mode-locking technique. An alternate way which produces shorter pulses than those obtainable by mode-locking in the 10  $\mu\text{m}$  wavelength range is to generate sideband frequencies by a fast amplitude modulation and to subsequently filter out the fundamental frequency. The amplitude modulation is performed by an optical gas-breakdown plasma, which truncates the incident 100 ns pulse in approximately 10 ps. As spectral filter hot  $\text{CO}_2$  gas, which is resonantly absorbing, gives an excellent pulse-to-background contrast ratio. In the hot  $\text{CO}_2$  gas the short pulse is generated by optical free induction decay, a physical process which is analogous to the free induction decay in nuclear magnetic resonance. The optical free induction decay was first used many years ago to generate short  $\text{CO}_2$  laser pulses. However, there were little applications until now. The main problem is the reproducibility of the truncation of a TEA-laser pulse by means of a reliable optical switch, sufficiently fast to truncate a TEA-laser pulse when it reaches the maximum power. Another point is the lack of commercially available high-power single-frequency TEA-lasers.*

*This work describes two new, improved and reliable optical free induction decay short-pulse laser systems, differing mainly in the pump laser and in the peak power of the generated pulse. Improved plasma shutters as optical switches operate at variable gas pressures. They are triggered by a laser-produced surface plasma or by an electrical high-voltage discharge. In this context we found new target materials for the surface plasma. The electrical discharge is initiated by the TEA-laser pulse via a new laser triggered spark gap. Furthermore, a TEA- $\text{CO}_2$  laser preionized by a novel surface-corona discharge was developed. This together with a low pressure cw-section forms a high-power hybrid- $\text{CO}_2$ -laser, which generates the required single-frequency pulses. An electronic control completes the systems as reliable working tools. Each of the two systems is capable to produce 10  $\mu\text{m}$  pulses as short as 30 ps.*

*Numerical calculations are performed to estimate the influence of various parameters on pulse shape and duration. Since a direct measurement of the time variation of the short pulses is not possible, we prove by means of an optical autocorrelation measurement with optical second harmonic generation that the expected pulse durations are achieved.*



## 1 Introduction

### 1.1 Survey

Today transversely excited atmospheric pressure (TEA)  $10\ \mu\text{m}$   $\text{CO}_2$  lasers find many applications in science and technology, e. g. Lidar, Dial, second harmonic generation (SHG) and optical pumping of far infrared (FIR) lasers. For many applications pulses shorter than those of TEA lasers are of interest, e.g. for optical pumping of FIR lasers. The aim of this work is a pulse-shaping technique which produces reproducible, well-defined 30 ps  $10\ \mu\text{m}$  pulses from a 70 ns TEA-laser pulse by optical free induction decay (OFID). For this purpose we built and tested several arrangements. The schematic of the most successful is shown in Fig. 1-1.

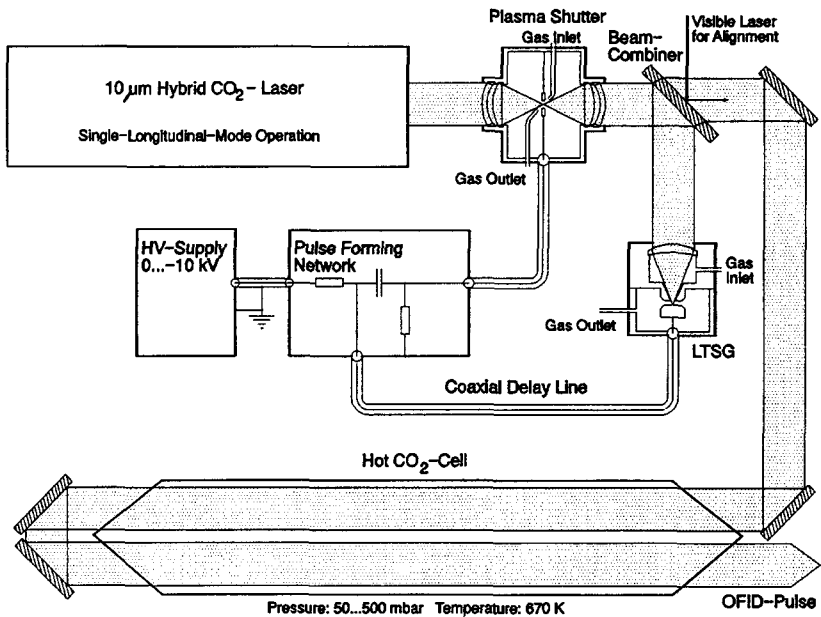


**Fig. 1-1:** Schematic of our most successful OFID-laser arrangement. The plasma shutter is triggered by an electrical discharge which is initiated by a laser-triggered spark gap (LTSG).

In this chapter we give an overview on TEA and short-pulse CO<sub>2</sub> lasers. The following chapters are devoted to a detailed description of the components of two optical free induction decay systems, which generate 30 ps CO<sub>2</sub> laser pulses. The two systems differ in the hybrid-laser applied and therefore in the power of the short pulse. Chapter 2 is devoted to the principle of the OFID. In chapter 3 the two hybrid-lasers applied are described and compared. The first TEA laser is a modified commercial laser, whilst the second was developed in our laboratory and is part of this work. The plasma shutter, an important tool in this short-pulse generation technique, is treated in chapter 4. In this study we have investigated and compared types of plasma shutters which differ in their trigger mechanism. The hot CO<sub>2</sub> cell as spectral filter is described in chapter 5. Finally chapter 6 is devoted to the calculated and measured characteristics of the short OFID laser pulses.

## 1.2 Transversely Excited CO<sub>2</sub> Lasers

In gas lasers the maximum output energy per pulse depends on the heat capacity of the laser gas, whose temperature rises with increasing input energy. The heat capacity and, consequently, the maximum output energy are proportional to the density of the gas. The pulse duration is also determined to a large extent by the gas pressure, since the relaxation times of the excited molecules become shorter at higher pressures. As a result the peak power is proportional to the square of the pressure [Witteman, 1987]. In order to obtain a high peak power the laser gas should be at a high pressure. However, at pressures above about 50 mbar a glow discharge constricts to an arc. Since arc discharges are unstable and not uniform they are not suited for efficient laser excitation of a gas. In addition, high voltages are required for axial laser systems with high gas pressure. This initiated the development of the transversely excited atmospheric pressure (TEA) CO<sub>2</sub> laser.

After transverse excitation had been introduced in the 540.1 nm neon laser at lower pressures [Leonard, 1965, 1967], French [Dumanchin and Rocca-Serra, 1969] and Canadian [Beaulieu, 1970] scientists independently reported transversely excited CO<sub>2</sub>-N<sub>2</sub>-He mixture lasers working at atmospheric pressure. After these early developments of the TEA CO<sub>2</sub> laser various improvements in excitation techniques were attempted. Beaulieu (1970) introduced an array of current-limiting resistors as pin electrodes to avoid a discharge in a single arc. Since the time of arc formation is finite [Johns and Nation, 1972], the formation can be inhibited by excitation with electric pulses whose duration is less than the arc-formation time. A pin-rod configuration without series

resistors yet with a shorter current pulse [Laurie and Hale, 1971] increased the efficiency. The disadvantage of these pin-rod configurations is the inhomogeneous excitation of the gas volume. In addition, only a part of the gas is heated during the discharge. This leads to substantial refractive-index variations and therefore results in a non-desired lens effect. This effect was minimized by the introduction of the helical pin-pin discharge configuration [Fortin et al., 1971]. However, the residual refractive-index variations still created the equivalent of a time-dependent long focal length diverging lens in the resonator.

A more uniform excitation of large volumes was realized by other discharge configurations [Dumanchin and Rocca-Serra, 1969; Laflamme, 1970]. A "double-discharge" arrangement forms a corona discharge between isolated trigger electrodes and the cathode. The resulting electrons in the vicinity of the cathode initiate the main discharge by lowering the discharge impedance. When the voltage applied between anode and cathode is reduced immediately after the current-pulse peaks [Pan et al., 1972] a uniform glow discharge between the electrodes can be achieved. An important modification of the double-discharge system was the introduction of trigger wires close to the cathode and parallel to the optical axis [Lamberton and Pearson, 1971; Pearson and Lamberton, 1972]. These wires were connected to the anode via a small trigger capacitor. When the spark gap fired, the storage capacitor was switched across the electrodes. A discharge between cathode and trigger wire developed until the trigger capacitors were charged. Direct ionization and UV radiation conditioned the gas mixture in a way, that a uniform glow discharge was achieved between anode and cathode. The electrodes in these devices were designed to produce a nearly uniform field in the discharge volume as first discussed by Rogowski (1923). The introduction of a so-called Rogowski cathode and a flat-grid anode with trigger pins behind the grid in combination with a Marx-bank voltage generator represented a significant improvement of double-discharge lasers [Richardson et al., 1973]. In this arrangement the corona discharge between the trigger pins and the grid developed rapidly into a number of arcs. The radiation of these arcs is rich in ultraviolet (UV) radiation and thus causes preionization of the main discharge volume. When the preionization reaches the optimum, another spark gap fires the main discharge. This permits the optimization of preionization. In the following years the role of volumetric photoionization and photoemission by a precursor spark discharge was studied extensively [Duley, 1976]. Seguin and Tulip (1972) passed the discharge current through a spark gap in series with the main discharge. The short-wavelength radiation from the auxiliary spark produced photoemission from the cathode as well as volume ionization in the gas. Therefore, a homogeneous glow discharge was achieved.

In all the UV-preionized systems described above the discharge starts with a low electron density ( $10^4 \text{ cm}^{-3} < n < 10^{18} \text{ cm}^{-3}$ ) [Witteman, 1987]. An important parameter describing the behaviour of the discharge plasma is the ratio  $E/N$  of the electric field  $E$  versus the gas density  $N$ . It gives information on the mean free path of an electron between two collisions. The larger the mean free path, the more energy the electron extracts from the field. When the  $E/N$ -ratio is sufficiently large the initial electrons are accelerated to an energy level sufficiently high to further ionize the discharge. Thus an avalanche ionization of the gas is possible until a quasi-steady-state electron density is reached. This type of discharge is called "self-sustained". On the contrary in a "non-self-sustained" discharge the applied  $E/N$  is relatively small and causes practically no further ionization. In this case the required ionization is produced by an external electron-beam (e-beam). Fenstermacher et al. (1971) used a hot-cathode electron gun for the generation of high energy (200 keV) electrons to initiate and sustain the discharge. A great advantage of this technique is the flexibility to match the  $E/N$  ratio to a specific gas mixture for an efficient vibrational excitation. Furthermore, such a system can be suited to generate relatively long laser pulses of about  $50 \mu\text{s}$  duration. Basov et al. (1971) used electron beam devices in a system with pressures up to 15 atmospheres. However, the e-beam devices are relatively complex compared to UV-preionized systems. For smaller volumes, as often required for single-mode systems, UV preionization is more suitable.

Although the previously described double-discharge UV-preionized systems are sophisticated, they are not optimized from the viewpoint of gas dissociation. Also the preionization is not uniform. These disadvantages can be avoided by the use of a corona discharge along a dielectric material on both sides of the electrodes. Hasson and Bergmann (1976) developed a knife-edge preionization technique on a dielectric sheet for the fast excitation of a nitrogen laser. Ernst and Boer (1978) pioneered a scheme producing a non-uniform high-voltage gradient at one end of a dielectric sheet for a rapid discharge TEA  $\text{CO}_2$  laser. A corona discharge in the gas near the dielectric produced a UV-preionization along the optical axis. This method was found to be superior to other types of self-sustained TEA lasers, because of the uniform preionization, the simplicity of the single discharge and its potential of relatively large electrode gaps up to 10 cm [Ernst, 1982]. A more detailed description of this technique will be given in Chapter 3.3.3 .

### 1.3 Short-Pulse CO<sub>2</sub> Lasers

The generation of short laser pulses is of great interest and has a wide range of applications in photochemistry, physics, biology and engineering [Kaiser, 1988]. During the past years remarkable progress in various types of short-pulse lasers has been made. Pulses as short as 6 fs have been produced in the visible [Fork et al., 1987]. However, the development of short-pulse lasers has mainly been concentrated on the visible or the near-infrared. Nevertheless, studies have also been devoted to the production of short mid- and far-infrared pulses, since they are suitable for investigations of intraband transitions in semiconductors, nonlinear vibrational effects in molecules, band-gap studies of high  $T_c$  superconductors and in laser chemistry. Mid-infrared laser pulses are also required for the optical pumping of far-infrared lasers.

Historically, cw laser action in CO<sub>2</sub> was first observed by Patel (1964). The first active mode-locked CO<sub>2</sub> laser was reported by Caddes et al. (1968). With a GaAs intracavity acousto-optic loss modulator they generated pulse trains with 5 ns pulse widths. Wood and Schwarz (1968) used SF<sub>6</sub> for passive Q-switching and thus produced pulse trains with 20 ns spikes and a peak power of 100 kW. McCoy (1969) reported continuous passive mode locking of 5 or 6 modes and 60 ns pulses. A rapid increase in maximum power from CO<sub>2</sub> lasers was achieved after the discovery that the CO<sub>2</sub> laser can be driven in a pulsed transverse-discharge configuration at pressures close to one atmosphere [Dumanchin and Rocca-Serra, 1969; Beaulieu, 1970]. This opened new aspects in the mid-infrared pulse generation. Gibson et al. (1971) applied hot CO<sub>2</sub> gas as saturable absorber for the passive mode locking of a transversely excited CO<sub>2</sub> laser and observed a pulse half-width of 4 ns. In the following years the transversely excited atmospheric (TEA) pressure laser was rapidly improved and resulted in transversely excited multi-atmospheric (TEMA) pressure CO<sub>2</sub> lasers. The increased pressure causes broadening and overlapping of the individual rotational laser lines and therefore yields a wider gain bandwidth. Mode-locked TEMA lasers generated 150 ps pulses [Alcock & Walker, 1974], while passive mode locked TEA lasers achieve a pulse duration of 400 ps by pulse compression with a saturable absorber [Feldman & Figueira, 1974]. Mode-locked lasers always show a train of short pulses. The extraction of a single pulse from such a pulse train is difficult. Thus only moderate contrast ratios are achieved. The application of a Pockels cell in a laser triggered Blumlein structure represents another technique which provides single 1 ns multiband pulses from TEA lasers [Figueira & Sutphin, 1974].

An entirely new pulse-shaping scheme to generate short CO<sub>2</sub> laser pulses was introduced by Yablonovitch and Goldhar (1974). They applied a laser-induced gas breakdown as active switching element for the generation of short pulses by optical free induction decay (OFID) in hot CO<sub>2</sub> gas. High-power pulses with an adjustable duration from 30 to 200 ps and an excellent contrast ratio can be produced this way [Kwok & Yablonovitch, 1977 a].

Shorter pulses than those produced by OFID require a faster switch. A system based on optically induced carriers in germanium to switch CO<sub>2</sub> laser radiation by means of a ruby laser was demonstrated for the first time by Alcock et al. (1975). The synchronous operation of a mode-locked Nd:glass laser and a TEA CO<sub>2</sub> laser with a germanium switch permitted to produce pulses of variable duration down to 5 ps [Jamison & Nurmikko, 1978]. An alternate approach is a dye laser-controlled Germanium reflection switch which injects a cw-CO<sub>2</sub>-laser into a mode-locked TEMA laser to give a pulse train with 200 ps pulses [Corkum et al., 1978]. The combination of two semiconductors, one to switch on the infrared reflection, a second to cut off the transmission, which are controlled by a colliding-pulse mode-locked dye laser yielded 9.5 μm CO<sub>2</sub> laser pulses as short as 130 fs, although at relatively low power [Rolland and Corkum, 1986]. These pulses correspond to only four optical cycles. They are the shortest pulses ever generated in the mid-infrared. Semiconductor-switched systems demand short-pulse lasers in the visible or near-infrared and provide only a moderate signal-to-background ratio.

## 2 OFID-System

### 2.1 Concept

The optical free induction decay (OFID) is a short-pulse generation technique different from mode-locking. In the OFID system an optical switch interrupts transmission with a cut-off time of a few ps. This can be regarded as a fast amplitude modulation, which causes sidebands in the frequency domain. An appropriate spectral filter rejects the frequency of the original laser pulse. Thus, a short laser pulse leaves the filter. As optical filters Yablonovitch (1975) suggested the Michelson interferometer, the Fabry-Perot etalon, the grating monochromator, a quarter-wave antireflection coating used in reflection and resonant-material absorbers. Among these hot CO<sub>2</sub> gas as resonant absorber exhibits the best rejection ratio. The short pulse is actually generated by optical free induction decay in CO<sub>2</sub> as demonstrated for the first time by Yablonovitch and Goldhar (1974). A cell containing the CO<sub>2</sub> gas is heated in order to populate the lower laser level and therefore to increase the absorption. If the cell is sufficiently long, the input beam is almost completely attenuated by linear absorption in the gas, i. e. contrast ratios better than 1:10<sup>6</sup> are possible. The output electric field can be regarded as a destructive interference between the input field and the electric field generated by the induced linear polarization in the absorber. Since the input beam is almost completely absorbed, the field generated by the medium is of the same amplitude as the input wave, but 180 degrees out of phase. If the input field is suddenly cut off, the molecular polarization in the hot CO<sub>2</sub> will continue to radiate for a time related to the transverse relaxation time, as its wave is no longer cancelled by destructive interference. The output pulse duration can be adjusted within certain limits, since the transverse relaxation time depends on the gas pressure.

The incident field has to be cut off in a time shorter than the transverse relaxation time. Therefore, a fast optical switch is required. It has been shown, that a high intensity CO<sub>2</sub>-laser-induced gas breakdown in the focus of a lens pair causes a frequency-shift of the transmitted beam due to the rapid growth of the initial plasma [Yablonovitch, 1973]. Once the plasma is initiated, the neutral gas ionizes rapidly. This changes the refractive index from originally unity in the neutral gas to zero when the critical electron density in the ionized gas is reached and, therefore, the transmission of the beam is stopped. Since the refractive index varies with space and time during the plasma

forming process, a phase and amplitude modulation with an asymmetric spectrum is produced [Yablonovitch, 1974 a]. Kwok and Yablonovitch (1977 b) labeled such a device as "plasma shutter". Therefore, a suitable switch for this pulse-shaping technique was found. Fig. 1-1 (cf. p. 5) shows the scheme of a complete OFID short pulse laser system.

## 2.2 Principle of Optical Free Induction Decay

The OFID is the optical analogue of free induction decay (FID) [Hahn, 1950] in nuclear magnetic resonance (nmr) [Rabi, 1937]. Basically OFID is quite simple: It is just the radiation emitted by molecules after they have been excited by a pulse [Shoemaker, 1978]. The name stems from nmr, where a sample of nuclear spins is first excited with a radio-frequency pulse. Subsequently the spins precess freely in the static magnetic field  $H_0$ . This free precession induces an oscillating voltage in a pickup coil used as a detector. The signal decays because the precessing spins get out of phase with each other owing to inhomogeneities in  $H_0$  [Hahn, 1950]. Thus, this nmr effect is called "free induction decay". While in nmr the two energy levels are connected via a magnetic-dipole transition, they are connected via an electric-dipole transition in the optical FID. Coherent transient phenomena observed in pulsed nmr have been investigated since the description of nuclear induction by Bloch (1946) and the experimental studies by Bloch et al. (1946). Later the development of the laser created considerable interest in optical analogues of the transient phenomena observed in pulsed nmr experiments on spin systems. Typical effects are optical nutation, optical free induction decay, photon echo, superradiance and self-induced transparency. These phenomena are discussed in detail by Allen and Eberly (1975) as well as by Shoemaker (1978). Experimentally OFID was demonstrated for the first time by Brewer and Shoemaker (1972) in an application of the Stark-pulse technique in  $NH_2D$ .

In the following we restrict ourselves to the basics of OFID. Some restrictions are assumed for a mathematical treatment: low-pressure gases, no solids, no effects arising from laser beam propagation through optically thick media. In experiments involving the interaction of radiation with gases the exact quantum mechanical state of each molecule in the gas is unknown. However, the distribution of molecules in various states is known. Therefore, a density matrix approach can be used rather than the Schrödinger



equation. The gas is described by a statistical ensemble whose members have differing wavefunctions. We restrict to two active levels  $a$  and  $b$  coupled by an optical radiation field. These levels are part of a manifold of other levels and communicate with them via collisional pumping and decay. Thus, a set of population matrix equations can be derived as shown in detail by Shoemaker (1978). In order to obtain applicable solutions of these equations special situations must be found, for which these equations simplify. Assuming that the upper- and lower-state decay rates are equal, i. e.  $\gamma_a = \gamma_b = \gamma$ , Shoemaker (1978) has derived the optical Bloch equations

$$\begin{aligned}\dot{u} &= (\Omega' - \omega_o) v - \gamma_{ab} u \\ \dot{v} &= -(\Omega' - \omega_o) u + \kappa E_o w - \gamma_{ab} v \\ \dot{w} &= -\kappa E_o v - \gamma[w - (n_a - n_b)]\end{aligned}\quad (2-1)$$

These are called "optical Bloch equations", because their fundamental form is exactly analogous to the Bloch equations of nmr [Bloch, 1946].  $u$  and  $v$ , when multiplied by  $\mu_{ab}$ , the transition dipole matrix element for the transition  $a \rightarrow b$ , are the in- and out-of-phase components of the polarization for molecules of given velocity  $v_z$ .  $w$  is the population difference  $\rho_{aa} - \rho_{bb}$ , where  $\rho_{aa}$  and  $\rho_{bb}$  represent elements of the density matrix. A molecule in motion with a speed component  $v_z$  in the optical axis sees a frequency  $\Omega' = \Omega - kv_z$ . The  $a \rightarrow b$  transition has a resonance circular frequency  $\omega_o = 2\pi\nu_o$ .  $\kappa E_o$  is the interaction strength, where  $\kappa = \mu_{ab} / \hbar$  and  $E_o$  is the amplitude of the pulse.  $n_a$  and  $n_b$  denote the number of molecules in levels  $a$  and  $b$ . The decay rates of the level populations are described by  $\gamma$  and  $\gamma_{ab}$  and are usually written as  $1/T_1$  and  $1/T_2$  respectively [Bloch, 1946].  $T_1$  and  $T_2$  are the longitudinal and transversal spin relaxation times, i.e.  $T_1$  is the relaxation of the population, whilst  $T_2$  is the relaxation of the induced dipole of the two-level molecule [Shimoda, 1984].

The optical Bloch equations describe the transition between two levels in a molecule whilst the Bloch equations of nmr describe transitions between the two levels of spin  $1/2$  particles. In nmr  $\omega_o$  is interpreted as  $-gH_o$  with  $g$  the gyromagnetic ratio and  $H_o$  the static magnetic field.  $\kappa E_o$  corresponds to  $gH_1$ , where  $H_1$  is a small magnetic field of frequency  $\Omega'$  applied at right angles to  $H_o$ . The quantities  $u$ ,  $v$  and  $w$  are then the components of the magnetization  $\vec{M} = (u, v, w)$  due to the nuclear spins in a coordinate frame rotating at frequency  $\Omega'$ .  $\gamma$  and  $\gamma_{ab}$  are usually written as  $1/T_1$  and  $1/T_2$  respectively.  $T_1$  and  $T_2$  are the longitudinal and transversal spin relaxation times.

The correspondence of the OFID with nmr permits the application of a model, known as vector model, as a geometrical picture for transitions between two levels in a molecule [Feynman et al., 1957]. When relaxation is neglected two vectors can be defined as  $\vec{M} \equiv (u, v, w)$  and  $\vec{\Omega} \equiv (\kappa E_0, 0, \Omega' - \omega_0)$ . Thus a gyroscope equation analogous to nmr formulates the geometrical picture for optical transitions:

$$\begin{aligned} d\vec{M}/dt &= \vec{M} \times \vec{\Omega} \\ \dot{M}_x &= \dot{u} = v(\Omega' - \omega_0) \\ \dot{M}_y &= \dot{v} = \omega\kappa E_0 - u(\Omega' - \omega_0) \\ \dot{M}_z &= \dot{w} = -v\kappa E_0 \end{aligned} \quad (2-2)$$

These equations imply that the vector  $\vec{M}$  precesses in a cone about an effective field  $\vec{\Omega}$ . This vector moves in an abstract vector space with the axes I, II, and III rather than in the physical space. The vector model visualizes the behaviour of the solutions of the optical Bloch equations.

Combining equations (2-2) and (2-1) and replacing  $\gamma$  and  $\gamma_{ab}$  by  $1/T_1$  and  $1/T_2$  respectively, yields equations analogous to the classical Bloch equations [Bloch, 1946]

$$\begin{aligned} \dot{M}_x &= (\vec{M} \times \vec{\Omega})_x - \frac{1}{T_2} M_x \\ \dot{M}_y &= (\vec{M} \times \vec{\Omega})_y - \frac{1}{T_2} M_y \\ \dot{M}_z &= (\vec{M} \times \vec{\Omega})_z - \frac{1}{T_1} (M_z - M_0) \end{aligned} \quad (2-3)$$

with  $M_0$  as the equilibrium polarization. The effect of the relaxation processes is an exponential decay of the induced polarization  $u$  and  $v$  by the rate  $1/T_2$ , whilst the population tends towards the equilibrium by the rate  $1/T_1$ . Thus the precession of  $\vec{M}$  about  $\vec{\Omega}$  is damped.

In the case of OFID the vector model gives a quite instructive picture. We assume an intense pulse of frequency  $\Omega = \omega_0$ , which starts at  $t_1$  and is turned off at  $t_2$ . Then a driving vector  $\vec{\Omega}$  is almost parallel to the I axis for all molecules. The  $\vec{M}$  vector for resonant molecules then precesses in a circle in the II-III plane. If the pulse duration  $t_2 - t_1$  fulfils  $\kappa E_0(t_2 - t_1) = \pi/2$ , the pulse is called a  $\pi/2$ -pulse. In this case  $\vec{M}$  precesses by  $90^\circ$ . For a pulse sufficiently intense,  $\vec{M}$  behaves identically for all molecules

and lies along the negative II axis. For times  $t > t_2$  we have  $\kappa E_o = 0$ . Consequently the driving vector  $\vec{\Omega}$  lies along the III axis. Each vector  $\vec{M}$  will therefore precess in the I-II plane. However, the  $\vec{M}$  vectors for molecules of different velocity will precess at different rates, because their  $\vec{\Omega}$ 's are different. This causes the vectors to fan out in the I-II plane. Since  $u$  and  $v$  are the in- and out-of-phase components of the oscillating dipole moment for some velocity group  $v_z$ , the direction of  $\vec{M}$  in the I-II plane shows the phase of the induced dipole moment with respect to the optical field. At time  $t = t_2$  all the vectors are in phase with each other, because they are all excited by the same optical field. Thus, the electric polarization  $\vec{P}$  is a maximum, and the system will radiate strongly an OFID signal, which is coherent and emitted in the same direction as the incident beam. The fanning out of the  $\vec{M}$  vectors is called "Doppler dephasing". It has nothing to do with collisional relaxation, as in this theory collisions have been neglected.

We have to mention the above simplification does not hold in our short-pulse laser arrangement, as the typical operating pressure of the hot CO<sub>2</sub> gas absorber is 100 mbar or higher. At this pressure collisions can not be neglected, since the absorption line is clearly pressure broadened. Furthermore, the absorber is optically thick and propagation effects in such a medium have to be taken into account. Therefore, the optical Bloch equations (2-1) are not valid unrestricted for a quantitative discussion of the OFID in the hot CO<sub>2</sub> gas absorber. Nevertheless, they give a quite instructive picture for the transient phenomena. In the next chapter we discuss a classical model suited to describe the behaviour of a gas near an absorption line.

### 2.3 Linear System Analysis

For a linear system analysis we assume at time  $t=0$  an incident CO<sub>2</sub> laser pulse whose duration is much longer than the switching time at time  $t=0$ . The incident laser oscillating at the frequency  $\nu_o$  has an electric field  $E_o(t)$ . The electric field  $E_{sw}(t)$  transmitted through the switch can be approximated by a falling step function

$$\begin{aligned} E_{sw}(t) &= [1-H(t)] E_o(t) \\ E_o(t) &= E_o \exp(i2\pi\nu_o t) \end{aligned} \quad (2-4)$$

$H(t)$  is Heaviside's unit step function according to the notation of Bracewell (1965). The Fourier transform of this field after switching is given by

$$\begin{aligned}
 E_{sw}(\nu) &= \int_{-\infty}^{\infty} [1-H(t)] \cdot E_o(t) \cdot e^{-2\pi i \nu t} dt \\
 &= \int_{-\infty}^0 E_o \cdot e^{i2\pi (\nu_o - \nu)t} dt \\
 &= \frac{E_o}{2\pi i(\nu_o - \nu)}
 \end{aligned} \tag{2-5}$$

After passing a filter with the spectral transmission  $G(\nu)$  the Fourier transform  $E_{out}(\nu)$  of the output electric field can be described by

$$E_{out}(\nu) = E_{sw}(\nu) \cdot G(\nu) \tag{2-6}$$

and thus we find by using equation (2-5)

$$E_{out}(\nu) = E_o \cdot \frac{G(\nu)}{2\pi i(\nu_o - \nu)} \tag{2-7}$$

Therefore, it is possible to produce short pulses of arbitrary shape and phase variation if an appropriate spectral filter  $G(\nu)$  and a suitable switch can be found [Yablonovitch, 1975]. As mentioned before, Yablonovitch (1975) proposed the Michelson interferometer, the Fabry-Perot etalon, the grating monochromator, a quarter-wave antireflection coating used in reflection and resonant-material absorbers as optical filters. Each of these filters has a specific transmittance function  $G(\nu)$ . In this study we can restrict our consideration to the resonantly absorbing hot CO<sub>2</sub> gas, because it has proven to be the optimum filter for short-pulse generation.

The optical Bloch equations (2-1) used to explain the OFID are valable for optically thin media, and also propagation effects have been neglected. However, hot CO<sub>2</sub> gas is an optically dense medium which is resonantly absorbing. Thus, another model to describe the refractive index of such a dense gas near an absorption line is needed. The classical model of the damped oscillator excited by an external field gives results equivalent to the correct quantum mechanical theory in the case of a two level absorption process. In this model one assumes a polarized electric field

$E = E_0 \cdot \exp[2\pi\nu t]$  and  $N$  molecules per unit volume as well as that each of these molecules behaves as a harmonic oscillator. The electric field of the incident light wave polarizes the CO<sub>2</sub> gas molecules, producing oscillating dipole moments. The acceleration of the oscillating charges radiates new waves of the field. This new field is interfering with the incident field and produces a changed field which is equivalent to a phase-shifted original wave [Feynman et al., 1964].

Solving the Maxwell equations for a dielectric with polarization  $\vec{P}$  and introducing the absorption length  $\alpha \cdot l$  (in Nepers) and the transverse relaxation time  $T_2$  yields the spectral transmission  $G(\nu)$  as given by Yablonovitch and Goldhar (1974)

$$G(\nu) = \exp \left[ -\frac{\alpha l}{2(1 + i(2\pi\nu - 2\pi\nu_0)T_2)} \right] \quad (2-8)$$

Here  $l$  denotes the length of the cell and  $\alpha$  is the absorption coefficient.  $T_2$  denotes the transversal relaxation time. It is related to the homogeneous linewidth  $\Delta\nu_H$  by

$$T_2 = \frac{1}{\pi\Delta\nu_H} \quad (2-9)$$

Abrams (1974) experimentally found the empirical relation for the 10P(20) laser transition at 10.6  $\mu\text{m}$  wavelength

$$\Delta\nu_H = 7.58 \cdot p_{\text{Torr}} [300/T]^{1/2} \text{ [MHz]} \quad (2-10)$$

where  $p_{\text{Torr}}$  is the pressure in Torr and  $T$  the absolute temperature. A more common formula for the P-Branch of CO<sub>2</sub> was given by Robinson and Sutton (1979) for the rotational quantum number  $J$  in the range  $0 \leq J \leq 40$

$$\Delta\nu_H = 22.79 \cdot (7.52 - 0.059 \cdot J) p_{\text{Torr}} T^{1/2} \text{ [MHz]} \quad (2-11)$$

We know from eqs. (2-7) and (2-8) the output spectrum of a falling step function passing the absorber gas. The electric field amplitude of the output pulse in time is given by the inverse Fourier transform of equation (2-7). Yablonovitch and Goldhar (1974) derived and illustrated an analytical solution for the normalized electric field amplitude of the output pulse

$$E_{out}(t) = E_o \cdot \left[ \exp\left(-\frac{\alpha l}{2}\right) - \exp\left(-\frac{t}{T_2}\right) \cdot \sum_{m=0}^{\infty} \left[\frac{2t}{\alpha l T_2}\right]^{m/2} J_m(y) \right]$$

with  $y = [2\alpha l / T_2]^{1/2}$  (2-12)

$J_m(y)$  is the Bessel function of first kind of order  $m$ . Input pulses which are more realistic than a falling step require numerical solutions. They are presented in section 6.1.

### 3 Single-Longitudinal-Mode Hybrid 10 $\mu\text{m}$ CO<sub>2</sub> Laser

#### 3.1 Single-Longitudinal-Mode Operation

In an open optical resonator only certain forms of the electromagnetic field show low loss. These field distributions are called modes of the cavity. In a first approximation these modes represent transversely electromagnetic (TEM) fields. For this type of mode both the electric and magnetic field of the electromagnetic wave are orthogonal to the optical axis. The notation for the description of such a mode is TEM<sub>nmq</sub>. Here q indicates the longitudinal mode number, whilst n and m represent the transverse mode numbers. The latter describe the light intensity distribution in a plane perpendicular to the laser beam. However, for a complete description of a mode the longitudinal mode index q is also needed. The frequency difference of two adjacent longitudinal modes with  $\Delta q = 1$  is  $\Delta\nu = c / 2L$ . For a cavity length of 2.3 m this separation is 65 MHz. The separation of the modes with identical q and different n and m depends on the resonator configuration. It is of the order of a few MHz. It vanishes for frequency degenerate modes e.g. in a confocal resonator [Kneubühl and Sigrist, 1991]. The emission line width of a TEA CO<sub>2</sub> laser is pressure broadened to about 3 GHz. Since the pulsed CO<sub>2</sub>-laser is a high-gain system, it has the tendency to oscillate on several longitudinal modes TEM<sub>00q</sub> and transversal modes TEM<sub>nmq</sub>, (n,m)  $\neq$  (0,0), simultaneously. This results in interference effects or "beats" at the difference frequencies [Siegman, 1986]. Mode-beating can be detected by any square-law photodetector whose response time is sufficiently short. For many applications the temporal power variation is undesirable. Therefore single-mode operation is required. An aperture in the cavity is adjusted to provide minimum loss for the longitudinal or fundamental modes TEM<sub>00q</sub>, but a high attenuation of the transversal or higher-order modes TEM<sub>nmq</sub>, where n,m  $\neq$  0. Fig. 3-1 (p. 20) shows two subsequent pulses of our TEA CO<sub>2</sub> laser operating in several longitudinal modes TEM<sub>00q</sub> simultaneously. Hence, they show spontaneous mode-locking. Since phases as well as amplitudes of these longitudinal modes vary from pulse to pulse, a random temporal intensity profile results, although the average energy remains constant. This situation is called "mode-coupling" while the term "mode-locking" is referred to those situations, where the different modes are all in phase or nearly in phase and thus produce a train of short pulses [Siegman, 1986]. In order to eliminate this modulation of the laser power single longitudinal mode (SLM) operation is required. Various attempts have been made to achieve this goal. It was found that a cell with 0.7 Torr SF<sub>6</sub> gas placed within the cavity of a laser operating

at 350 Torr acts as a mode selector [Nurmikko et al., 1971]. SLM operation was also obtained by means of an uncoated germanium flat as an intracavity etalon for laser gas pressures up to 350 Torr [Weiss and Goldberg, 1972]. At higher pressures additional longitudinal modes TEM<sub>00q</sub> were present.

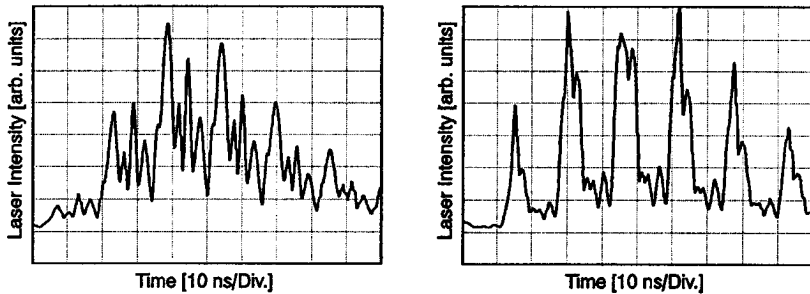


**Fig. 3-1:** Two subsequent pulses of a TEA-laser oscillating simultaneously in several longitudinal modes TEM<sub>00q</sub>. The low-pressure cw-section is switched off. This results in spontaneous mode-locking with random temporal intensity profile from shot to shot.

A new method for achieving single-frequency output at an operating pressure of 500 Torr was introduced with the hybrid laser [Gondhalekar and Holzhauer, 1973]. In this construction, a low-pressure continuous wave (cw) gain section with narrow gain width is incorporated in the cavity together with the pulsed high pressure discharge section. A similar arrangement combining a double-discharge TEA-laser and a low pressure cw section was reported to change considerably the laser-pulse characteristics [Girard, 1974]. The low-pressure section with a bandwidth narrower than the longitudinal-mode spacing provides an extra gain and an extra spontaneous radiation level for one particular mode. Two regimes of operation are observed in a hybrid-CO<sub>2</sub>-laser [Girard, 1974]:

- a) The cw section operates under the lasing threshold,
- b) The cw section works over the lasing threshold.

In case a) the fast pulse of pumping current in the TEA section creates to a gain-switched [Siegman, 1986] giant pulse similar to that of a simple TEA section. However, no spontaneous mode-locking occurs and a smooth pulse followed by a long tail is



observed. This long tail is due to repumping of the upper laser level by collisions between vibrationally excited N<sub>2</sub> molecules and non-excited CO<sub>2</sub> molecules. The delay between the start of the current pulse and the laser output decreases with increasing discharge current in the cw section because the threshold gain is reached earlier [Girard,1974].

In case b) where the cw laser gain is above the threshold already before the TEA excitation, the pulse builds up even earlier than in case a). In fact, there is no time to build up the high gain required for a gain switched pulse. Instead, a single mode pulse with a relatively slow rise-time, a smaller amplitude and a long duration is obtained. The pulse energy, however, is the same in both cases. Fig. 3-2 illustrates the two different pulse shapes.

Depending on the cavity length and the pressure in the cw section two adjacent longitudinal modes may have approximately the same gain. The resulting pulse is a two-mode-beating pulse train as illustrated in Fig. 3-3A. In order to avoid this situation and to obtain single longitudinal-mode operation as shown in Fig. 3-3B, it is necessary to change the cavity length a fraction of a half-wavelength in order to shift one longitudinal mode to the maximum of the gain curve of the hybrid laser.

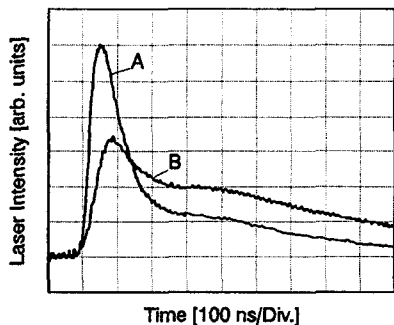


Fig. 3-2: Single mode pulses TEM<sub>00q</sub> from a hybrid-CO<sub>2</sub>-laser. Trace A is the gain-switched giant pulse produced when the cw-section operates under the lasing threshold. Trace B is obtained with the cw-section lasing over the threshold with a power of approximately 3 W. The peak power is lower than in trace A, however, the total pulse energy is the same in both cases. In case B note that in reality the laser starts to oscillate several tens of nanoseconds earlier with respect to the discharge.

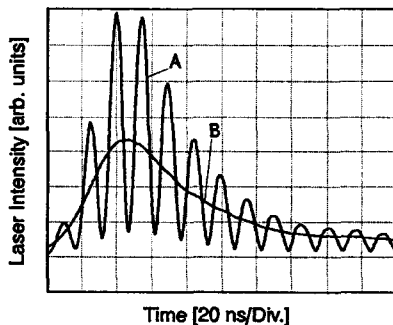


Fig. 3-3: Two hybrid-CO<sub>2</sub>-laser pulses of the same energy. Trace A is a two-mode-beating pulse train obtained by detuning the cavity length by a quarter wavelength. The strong modulation indicates, that the two modes have almost the same amplitude. Adjusting the cavity length reduces the gain of one mode relative to the other and therefore the modulation diminishes. Trace B is the desired single-mode pulse.

A different approach to achieve a SLM-TEA laser operation is to shorten the cavity length to enlarge the longitudinal mode spacing. It has been demonstrated that a TEA laser with a cavity length of only 150 mm is suited for SLM operation [Ernst, 1977]. In this case the cavity length has to be tuned to shift the mode into the centre of the gain profile. Naturally this technique is limited to low-power applications. Another way of mode control in a TEA CO<sub>2</sub> laser is injection locking. This was analysed and demonstrated by Lachambre et al. (1976). Two different types of injection-locking behaviour exist [Siegman, 1986]. In the case of true injection locking a weak monochromatic signal is injected into the resonator of another self-sustained oscillator, whose free-running frequency is within a narrow locking range of the injected frequency. In the case of the injection-locked TEA laser a weak signal of a master oscillator is injected into a pulsed high-power oscillator and establishes the initial conditions from which the pulsed oscillation starts to build up.

Parameter	Laser I	Laser II
Resonator Length	2.3 m	2.3 m
Discharge Volume	1.0 l	0.3 l
Storage Capacitor	2 x 75 nF	2 x 75 nF
Operating Voltage	40 kV	30 kV
TEA Discharge Length	2 x 46 cm	2 x 40 cm
CW Discharge Length	45 cm	70 cm
Pulse Energy ( $TEM_{00q}$ , 10P(20))	0.3 J	1.0 J
Peak Power (SLM)	1.5 MW	7 MW
Repetition Rate	0.5 Hz	2 Hz
Total Gas Flow	12 l/min	4.5 l/min
Gas Mix (CO <sub>2</sub> : N <sub>2</sub> : He)	10:6:84	32:7:61 (low tail) 31:11:58 (high energy)

Table 3-1: Characteristic data of our two hybrid 10  $\mu\text{m}$  CO<sub>2</sub> lasers

However, in this case the injected signal is too weak or too far off-resonance to really "lock" the oscillator as in the previous case [Siegman, 1986]. Although the expression "injection locking" is commonly used for both types of lasers, the behaviour is quite different. Consequently, Siegman (1986) refers to the pulsed injection locking more accurately as "injection seeding" of the pulsed oscillator. The injection method requires two independent lasers, a cw-CO<sub>2</sub> and a TEA CO<sub>2</sub> laser, whose frequencies have to be matched to produce stable SLM pulses. This matching however results in a reduction of the obtainable peak power, because the short buildup time inherent in the production of such pulses lowers the gain-switching effect. Thus, a condition has to be found to compromise the injection and gain-switching effects [Tashiro et al., 1984]. For our OFID-systems we have built two hybrid-CO<sub>2</sub>-lasers, since hybrid lasers with pulse energies above 100 mJ are not available commercially. These lasers are described in the following sections 3.2 and 3.3. For comparison, we have summarized their characteristic data in Table 3-1 (p. 22).

### 3.2 Hybrid-CO<sub>2</sub>-Laser-System I

The first hybrid CO<sub>2</sub> laser system we have built consists of two Lumonics TEA 100-2 CO<sub>2</sub> discharge tubes with a discharge cross section of approximately  $3.3 \times 3.3 \text{ cm}^2$  and a total discharge length of 92 cm. The required preionization is performed by a double discharge technique similar to that introduced by Seguin and Tulip (1972), where the main discharge current passes through a series spark gap. The discharge can be described in three phases: the over-voltage, the preionization and the main-discharge phase. The firing of the spark gap impresses a rapidly decreasing voltage on the preionization pins versus the cathode. Since the laser gas is neutral and non-conducting between pulses, the voltage in the pin-cathode gap rises above the DC breakdown voltage and breaks down along the entire length of the electrode. This is the start of the preionization phase. The discharge current charges the cathode capacitor and produces the preionization. The generated UV-radiation is emitted into the interelectrode volume through the holes in the mesh-cathode. An arc from each pin to the cathode terminates the preionization phase and passes the current for the main discharge to the cathode. A self-sustained discharge from the cathode to the anode excites the laser gas. The main discharge has to be terminated before a bright arc can form. The duration of the main discharge phase is largely determined by the electrical parameters of the discharge circuit. Nevertheless, the geometry of the laser and the gas

mixture have a strong influence on the previous phases and, therefore, on a discharge suited for laser excitation. The relatively large discharge volume of 1.0 l permits pulse energies up to 10 J in multimode operation. However for reliable operation of the OFID-system a single fundamental mode TEM<sub>00q</sub> is required. For maximum energy extraction from the excited gas into a single TEM<sub>00q</sub> mode a resonator type with a large mode volume and a discrimination against higher-order transverse modes must be used. This claim can only be fulfilled by the unstable resonator [Siegmán, 1974]. In a hybrid laser this requires a low-pressure gain cell with the same large cross section as the TEA laser.

This may be accomplished by a transversely excited (TE) low-pressure section rather than by a continuous axial discharge because the pulsed discharge needs no cooling. In a first approach we applied a Lumonics Model 531 pulse-smoothing option, which consists of a low-pressure TE pulsed discharge tube. The active length is 0.36 m and the cross section is 4 x 4 cm<sup>2</sup>. The trigger signal of the TEA section has to be delayed versus that of the TE section by approximately 450  $\mu\text{s}$ . Unfortunately, this system worked unsatisfactory with respect to single longitudinal mode operation.

For this reason, we started another approach by means of a stable resonator, with a smaller mode volume and, consequently, reduced pulse energy. Fortunately, this permits the use of a continuous wave (cw) low-pressure gain cell as reported by Girard (1974). Therefore, we have constructed a cell consisting of a water-cooled glass tube with an inner diameter of 18 mm and a discharge length of 0.45 m. It operates below the lasing threshold in order to produce a gain-switched pulse as mentioned in section 3.1. Adjusting the cavity length permits single TEM<sub>00q</sub> mode operation.

The stable resonator of the hybrid laser system I is formed by a concave ZnSe outcoupling mirror of curvature radius 20 m, and a plane diffraction grating. This grating permits line-tuning of the laser. If the dispersive properties of the grating are ignored, this configuration is equivalent to a planoconcave resonator [Chodzko et al., 1973]. An adjustable aperture close to the grating selects the TEM<sub>00</sub> mode to oscillate. Brewster windows seal the cw and TEA sections and provide a highly polarized output beam.

The described system works satisfactory, except that the output energy is relatively small compared to the large excited volume. A higher pulse repetition rate would also be agreeable for many applications. For this reason we designed and built a new hybrid-laser in our laboratory with greatly improved performance. This laser is described in the following section.

### 3.3 Hybrid-CO<sub>2</sub>-Laser-System II

#### 3.3.1 System Design

In order to overcome the disadvantages of the hybrid-laser described above we developed a new system including a cw-stage and a TEA laser optimized for single-mode operation. Since TEM<sub>00q</sub> mode operation is required, the TEA discharge cross section is reduced to 20 x 20 mm<sup>2</sup>. In order to achieve good beam quality the discharge needs to be homogeneous and show no streamers. This requires a homogeneous volume preionization and a low-inductance discharge circuit yielding a short current rise time and a rapid energy deposition in the laser gas. The discharge current has to be terminated before streamers can form and heat the gas locally. This would result in a temporal and local refractive-index variation influencing the beam quality. Among the UV-preionized systems described in section 1.2 the dielectric corona-discharge preionization (silent discharge) is best suited to fulfil these requirements. In addition, this preionization type yields a discharge scheme minimizing the CO<sub>2</sub> gas decomposition rate [Marchetti et al., 1983]. The CO<sub>2</sub> dissociation with concomitant formation of molecular oxygen gives rise to strongly attaching neutrals and negative ions which results in subsequent loss of discharge stability. In order to achieve a low-inductance discharge circuit we apply a Blumlein-type scheme well known from nitrogen lasers. The low-pressure section is excited by a continuous longitudinal discharge in a glass tube 70 cm long. The inner diameter of the tube is 16 mm. The glass tube is water cooled because an electric power up to 50 W can be put into the discharge. The laser cavities of the cw and TEA section are sealed with NaCl Brewster windows. A welded steelbox encloses the TEA-laser section to suppress electrical noise generated by the fast high-current discharge. Care has to be taken to avoid groundloops. In the following we discuss the uniform field electrodes and the dielectric corona preionization in detail.

#### 3.3.2 Uniform-Field Electrodes Design

For manufacturing purposes the TEA laser is split into two sections, each with a discharge length of 40 cm. The most difficult part is the fabrication of electrodes with

a uniform field distribution. A uniform energy loading of the active gas medium is important in order to gain high output power. This can be achieved by special contours of the electrodes. Several authors have tried to solve this problem. Rogowski's (1923) profile was initially developed for testing dielectric materials whilst Chang (1973) designed an analytic profile for TEA-laser and high-voltage applications. With the introduction of transversely excited gas lasers Rogowski's (1923) as well as Chang's (1973) profiles were commonly used as uniform-field electrodes until the introduction of Ernst's profiles (1984). The advantage of the Ernst's profiles is their minimum width for a given discharge width. The width of the electrodes is an important characteristic for UV-preionized systems. It permits to locate the UV source as close as possible to the discharge volume. Furthermore, the electrode inductance is reduced and the current rises faster. Mathematically Ernst's profiles are derived from Chang's by adding a third term in the conformal transformation, which results in

$$\zeta = w + k_o \sinh w + k_1 \sinh 2w \quad (3-1)$$

where  $\zeta = x + iy$  and  $w = u + iv$ .  $x$  and  $y$  are the space coordinates whilst  $u$  and  $v$  indicate the flux and potential functions. The profile of the corresponding equipotential surface for  $|v| < \pi$  is given by

$$\begin{aligned} x &= u + k_o \sinh u \cos v + k_1 \sinh 2u \cos 2v \\ y &= v + k_o \cosh u \sin v + k_1 \cosh 2u \cos 2v \end{aligned} \quad (3-2)$$

where  $u$  is the curve parameter. With these relations the profiles are not uniquely determined. The form of the profile as well as the electric-field strength distribution are determined by the three independent variables  $k_o$ ,  $k_1$  and  $v$ . Ernst (1984) calculated these variables according to Chang (1973) and represented the electric field as a power series expansion near  $u=0$ . The terms of odd power are missing due to symmetry. Ernst found as optimum for the best field uniformity

$$v = \frac{\pi}{2} \quad \text{and} \quad k_1 = \frac{1}{4} [1 - (1 - k_o^2)]^{1/2} \quad (3-3)$$

The addition of one extra term in Chang's profile expansion according to Ernst reduces the electrode width by roughly 15 %. The uniformity of the field distribution is also drastically improved (Ernst, 1984). In Fig. 3-4 the electrode profiles for  $k_o = 0.02$  according to Rogowski, Chang and Ernst are plotted for comparison. Ernst also added

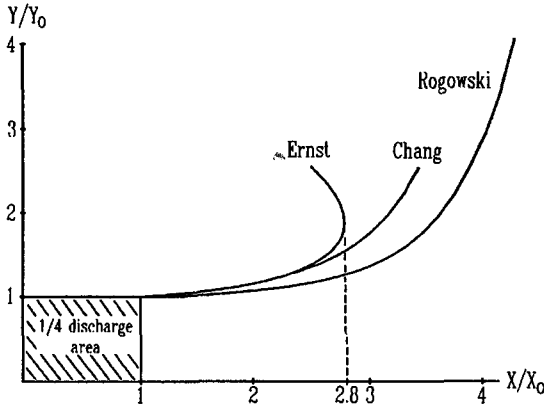


Fig. 3-4: Electrode profiles for  $k_0 = 0.02$  according to Rogowski, Chang and Ernst.

a fourth term,  $k_2 \sinh 3w$ , in (3-1) and used the extra parameter  $k_2$  for optimizing the field uniformity. He tried further improvement of the uniformity and compactness by adding even more terms in (3-1). However, he noticed that this does not give any substantial improvement over what has already been achieved. The shape and the relation between electrode gap and electrode width of the Ernst's profiles is determined by the parameter  $k_0$ . We have chosen  $k_0 = 0.02$  to obtain a square discharge. Subsequently, we have scaled  $x$  and  $y$  for  $y_0 = 10$  mm, which corresponds to an electrode gap of 20 mm. The width of the electrode can be calculated by the relation,  $\partial x / \partial u = 0$ . Therefore  $u_{\max}$  is given by

$$u_{\max} = \frac{1}{2} \cdot \operatorname{arccosh} \frac{2}{1 - (1 - k_0^2)^{1/2}} \tag{3-4}$$

By substituting  $u_{\max}$  in (3-2) the half electrode width  $x_{\max}$  and the electrode height  $y_{\max}$  can be calculated. In our case the maximal width of the profile is 55.97 mm. The profile is fabricated on a computerized numerical control (CNC) milling machine. A brass bar is first milled flat on bottom and top. Before the Ernst profile is milled on the top, the brass bar is tempered in order to minimize twisting by internal strain. Various methods of milling the calculated profile can be applied. A milling tool of the desired profile can be manufactured. With this tool the profile is produced in a single roundtrip on the milling machine. This is the fastest method to produce a number of electrodes.

However, for the manufacture of electrodes wider than a few millimeters expensive tools are required. Furthermore, the cutting speed of such a tool is small close to the axis, yet fast near the outer diameter. A different approach is the application of a standard spherical milling tool, commercially manufactured with various diameters. With this tool the electrode profile is produced by an iterative milling process. The number of round trips depends on the surface smoothness desired. We have chosen the latter method, since it is most suitable for producing a few pieces. The maximal tool displacement  $\Delta w$  between to round trips depends on the radius  $R$  of the milling tool and the maximum tolerated local deviation  $\Delta S$  of the spherical tool from the desired surface. It can be approximated by the equation

$$\Delta w \approx 2(2\Delta SR)^{1/2} \quad (3-5)$$

A computer program automatically calculates the coordinates for the milling machine and optimizes the number of round trips according to (3-5). For a surface roughness corresponding to N7 (ISO 1302) the deviation  $R_a$  average peak to valley is  $1.6 \mu\text{m}$  whilst  $\Delta S$  is approximately  $2 \mu\text{m}$ . This surface texture is achieved with a displacement  $\Delta w$  of  $0.4 \text{ mm}$ . Under these conditions as many as 82 roundtrips are required for an electrode of width  $55.968 \text{ mm}$ . After milling the electrode is polished. The final surface roughness achieved is N3, corresponding to  $R_a = 0.1 \mu\text{m}$ .

### 3.3.3 Dielectric Corona Preionization

As mentioned in section 1.2 the development of self-sustained discharges by application of UV radiation to preionize the laser gas has given rise to a number of sophisticated techniques. In fact, the choice of the preionizer is important from the standpoint of achieving optimized laser performance. Only a glow-discharge is capable of sufficient excitation of the laser gas. Normally, a glow discharge at atmospheric pressure is unstable and rapidly constricts to an arc. However, the arc develops in a finite time [Johns and Nation, 1972]. Therefore a glow-discharge at pressures of several atmospheres can be generated by producing a sufficient number of start electrons and by limiting the discharge duration. The starting electrons are provided by preionizing the laser gas. According to Palmer (1974) the minimum initial electron density required in the discharge volume of a TEA CO<sub>2</sub> laser is  $n_{e_0} \geq 10^4 \text{ cm}^{-3}$ . Also this initial density is relatively low, a high quasi-steady-state electron density is reached by avalanche



ionization in the discharge. A fundamental parameter which governs the discharge plasma in the quasi-steady-state regime is the ratio  $E/N$ , the electric field  $E$  versus the gas density  $N$ . The applied electric field accelerates the initial electrons to an energy level sufficient to further ionize the gas and thus to self-sustain the discharge. This implies a higher  $E/N$  ratio than in a non-self-sustained discharge, where the required ionization is produced by an external electron beam. The maximal current density in a homogeneous streamer-free glow discharge is limited by the initial electron density  $n_{e_0}$ . Hasson and Bergmann (1980) found a maximal gain for the ratio of the electron density  $n_e$  corresponding to a local current versus preionization electron density  $n_{e_0}$

$$n_e / n_{e_0} \leq 10^8 \quad (3-6)$$

In order to achieve a high laser power a high current density and a high initial electron density by preionization is required. Furthermore, a sufficiently high initial electron density permits a smaller  $E/N$  ratio. Therefore, the electron energy can be optimized to improve the excitation efficiency. For electrons of an energy of 1 to 2 eV the cross section for exciting the upper laser level in CO<sub>2</sub> reaches a maximum [Lowke et al., 1973]. With increasing electron energies bend and stretch modes as well as electronic states are excited. With energies higher than 10 eV the gas can be ionized. For electron energies below 1 eV the energy is lost to elastic collisions and to stretch and bend modes coupled to the lower laser level. Lowke et al. (1973) calculated the operating  $E/N$  ratio for a self-sustained glow discharge to be approximately  $10^{-16} \text{ V cm}^2$ . Depending on the gas mix, between 60 and 80 % of the power can be put into the upper laser level if the adequate  $E/N$  ratio is chosen. Egger et al. (1976) investigated the spatio-temporal development of a self-sustained discharge experimentally as well as analytically. They found that a uniform preionization is necessary to obtain a homogeneous glow discharge without streamers. Discharge instabilities are due to a locally enhanced electron density, which causes local overheating and expansion of the gas. Since the preionization makes a high-pressure glow discharge possible and influences the transient behaviour of the discharge as well as the possible current density, the choice of an appropriate preionization technique is of utmost importance. A UV source is desirable which is uniform and extends over the area defined by the length of the electrodes and their separation.

The dielectric corona discharge (silent discharge) is the most successful technique to achieve this aim [Wittman, 1987]. The term "corona discharge" often refers to a phenomenon which occurs in a gaseous medium in the vicinity of an electrode with a small radius of curvature subjected to a high voltage. The high electric field along the

surface is distorted by the small radius of the electrode. If the local increase of field strength is sufficient the surrounding gas is ionized. The charge carriers thus produced drift to the opposite charged electrode. The resulting self-sustained discharge current is generally considerably smaller than in a glow discharge. Pearson and Lamberton (1972) placed a tungsten wire parallel to a pair of Rogowski electrodes, yet offset from their center line. Each end of the wire was connected to the cathode by a small capacitor. When a high-voltage pulse was applied to the main electrodes field emission from the wire induced a corona discharge between the wire and the anode. This discharge is limited in energy by the choice of coupling capacitors. Also this technique is simple, the UV illumination of the interelectrode volume is not quite homogeneous. Hasson and Bergmann (1976) developed another preionizing technique in a nitrogen laser using two knife edges on a dielectric material as corona electrodes. The advantage of this method is the production of UV close to the main electrodes. However, precise alignment of the knife edges is necessary. Furthermore, the strong field on the knife edges dissociates the laser gas. A further dielectric corona-preionization method was pioneered by Ernst and Boer (1978). A suitable dielectric sheet has an electrode on one side and is subjected to a high-voltage gradient across. The high electric field in the dielectric sheet produces a surface corona discharge in the surrounding gas. Basically the same technique was applied by Schwab and Hollinger (1976) and by Kälín and Vonesch (1983) in Blumlein-type N<sub>2</sub> lasers, where a fast current rise is required to prevent depopulation of the excited laser level by spontaneous emission. However, the observed streamerless glow-discharge was attributed to the minimized self-inductance in the discharge current loop rather than to the corona preionization. The dielectric corona preionization technique is most promising for uniform UV illumination between the main electrodes. Furthermore, the gas dissociation effects are minimized and the uniform streamerless discharge gives good optical beam quality. Also the dimensions of the preionizer for best operating conditions must be determined empirically, the construction remains relatively simple.

Since we decided to apply this dielectric corona discharge in our new TEA-laser, the mechanism of UV production is explained with the aid of Fig. 3-5 which shows a cross section of the laser cavity perpendicular to the optical axis. Our electrical arrangement resembles a Blumlein circuit similar to that designed by Ernst (1977). However, discrete doorknob capacitors are used instead of a stripline capacitor and the cavity is designed symmetric. Initially, both electrodes are charged to a positive high voltage. When the spark gap fires, the lower electrode voltage is reversed and this electrode acts as the cathode. The suddenly applied high-voltage pulse generates a rapidly rising

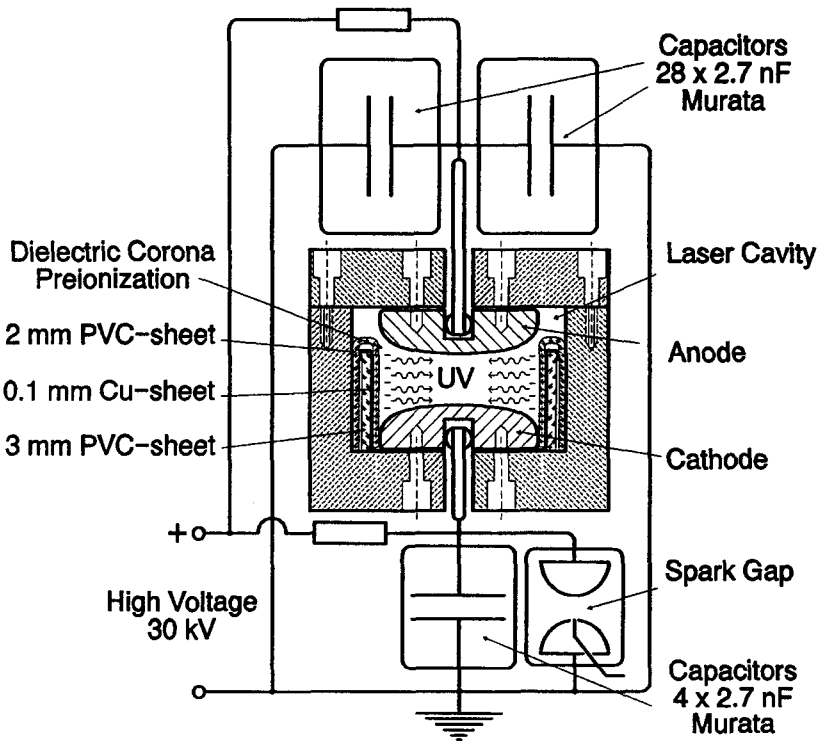


Fig. 3-5: Cross-section of the TEA-laser system II perpendicular to the optical axis.

electric field, which is uniform in the central part of the electrodes as explained in section 3.3.2. The cathode has an extension manufactured of copper sheets bent to align with the discharge volume on both sides. This extensions are surrounded by dielectric sheets to prevent a breakdown between the anode and the cathode extension. At the instant of spark-gap firing the dielectric sheets are exposed to a strong electric field and are charged on the surface (Fig. 3-5). The resulting displacement current depends on the capacity formed by the cathode extension, the dielectric sheet and the anode. The capacity of the dielectric sheet is inversely proportional to its thickness. A surface corona discharge produces ions and electrons in the surrounding gas. Whilst the ions are attracted by the dielectric surface, the electrons form streamers which rapidly develop into avalanches. The plasma produced on the surface of the dielectric sheet

extends over an area defined by the main electrode spacing and the main discharge length.

Beverly (1978) studied extensively the light emission from current surface-spark discharges. He found that the initial light emission is largely determined by the initial change rate of the current.

This requires a low-inductance driving circuit, since the initial current rise is

$$di/dt = V/L \quad (3-7)$$

where  $V$  represents the initially imposed voltage and  $L$  the inductance of the discharge circuit. From applications in nitrogen lasers the Blumlein-type discharge circuit is well known to fulfil this claim. The investigated spectrum for pure nitrogen contains UV radiation in the range from 100 to 200 nm whilst pure CO<sub>2</sub> shows small spectral light intensities. Babcock et al. (1976) measured the UV absorption in CO<sub>2</sub> gas. They found that photons in the relatively small spectral window from 117 nm to 124 nm and with wavelengths longer than 160 nm can penetrate sufficiently. For other wavelengths the gas is essentially black. From this result it is clear that both, the laser gas mixture and the gas pressure, strongly affect the behaviour of the discharge. Reduction of the nitrogen in the laser gas results in a lower pulse energy, since nitrogen repumps the upper laser level by collisions of the second kind, i.e. near resonant energy transfer, and is therefore responsible for the long tail of the laser pulse as explained in section 3.1.

For our short-pulse laser system a high peak power is desired rather than high energy partially contained in a long tail. Nevertheless, the nitrogen is responsible for the UV generation and herewith for the glow-discharge conditioning. For this reason the nitrogen content can be minimized in favour of the CO<sub>2</sub> content, yet it cannot be totally omitted. Other important parameters that affect the preionization and therefore the discharge characteristic are the thickness of the dielectric sheet, the material, the gap between the sheet and the electrodes, and the voltage applied. The dielectric function  $\epsilon$  of the dielectric sheet affects the distributed capacity of the cathode extension and the anode. Furthermore, the kind of dielectric influences the UV spectrum of the surface emission [Beverly et al., 1977]. The radiation emitted from a high-current density surface discharge is concentrated in the spectrum near 120 nm [Zaroslov et al., 1978]. It is therefore more efficient for the preionization of a CO<sub>2</sub> laser gas than a spark discharge. Since they measured a strong dependence of the spectrum on the dielectric material, Zaroslov et al. (1978) suggested impregnating the dielectric material with chemical elements which show strong lines in the required spectral range. A small

amount of the dielectric surface is evaporated by the surface discharge. The resulting impurities with a low ionization energy form electrons by absorption of photons in a single- or multiphoton process. Walter (1985) tested and compared five different dielectric materials in a corona preionizer for a CO<sub>2</sub> laser. He reported a maximum output energy difference of 25 % under the same operating conditions for macor (glass ceramic) as the best and for epoxy as the poorest dielectric. For the first time we used in our laser a 3 mm thick PVC sheet as a corona preionizer, since it offers an excellent breakdown-voltage and can easily be formed by thermal treatment.

### 3.3.4 Optical Resonator

The stable resonator is formed by plane mirror or alternatively a grating and a Ge outcoupling mirror of 10 m radius and 36% reflection. The cw section works below threshold under this conditions. At an operating pressure of 10 mbar the line width is about 50 MHz, whilst the longitudinal mode spacing of the 2.3 m resonator is 65 MHz. Thus, it is possible that two adjacent longitudinal modes fall within the gain profile of the cw cell and therefore grow to almost the same amplitude. Reducing the pressure in the cw cell results in a reduced gain. This could be compensated by a longer cell. However, this would increase the cavity length and give a smaller longitudinal mode spacing. In this ambiguous situation a compromise has to be found between operating pressure of the cw cell and total cavity length. For stable long-term operation it is inevitable to adjust the cavity length by a piezoelectric lead zirconate titanate (PZT) ceramic translator. Its aim is to move the axial modes with respect to the gain profile of the hybrid system. A translation of a half wavelength suffices to shift a longitudinal mode by a complete cycle. Proper adjustment of the PZT results in a smooth single frequency pulse as shown in Fig. 3-3B (p. 21), whilst a displacement of the outcoupling mirror by a quarter wavelength gives rise to two adjacent longitudinal modes with almost the same gain which results in strong two-mode beating (Fig. 3-3A p. 21). In practice the pulse shape has to be monitored from time to time to ensure that there is no mode beating. Although the resonator elements are spaced by super-invar rods and the laboratory temperature is almost constant, readjustment of the PZT is necessary all 15 to 20 minutes. This has probably to be attributed to a change of refractive index of the laser gas by a temperature change or a slight variation of the gas mix. The optical path  $W = n \cdot L$  in the resonator, where  $L$  is the cavity length and  $n$  the refractive index of the gas, changes with a refractive index variation  $\Delta n$  as  $\Delta W = \Delta n \cdot L$ . Therefore a change of refractive index  $\Delta n$  of less than  $4 \cdot 10^{-6}$  in the TEA section is identical to a

change of the cavity length by a quarter wavelength. This can cause mode beating until the cavity length is readjusted. Unfortunately, a refractive index change sufficient to change the cavity length a quarter wave easily occurs by a small change of the laser gas. The pressure of the TEA laser also varies with the atmospheric pressure. This represents another source of instability. The exact values of refractive indices are unknown at the CO<sub>2</sub>-laser wavelength. For an estimation of the order of magnitude we use the known data of the visible. For D light, i. e. the Fraunhofer designation of sodium arc at 589 and 592 nm wavelength the following refractive indices  $n_o$  at 0°C and 1013 mbar have been published by Gray et al. (1972):

CO <sub>2</sub> :	$n_o = 1.000451$
N <sub>2</sub> :	$n_o = 1.000297$
He:	$n_o = 1.000036$

The refractive index of the laser gas mixture is unknown, yet probably close to 1.0003 in the visible. Gray et al. (1972) also presents a formula by Biot and Arago which describes the dependence of the refractive index of a gas on pressure and temperature:

$$n(T, p) = 1 + (n_o - 1) \cdot \frac{T_o}{p_o} \cdot \frac{p}{T}$$

with:  $p_o = 1013 \text{ mbar}$ ,  $T_o = 273 \text{ K}$  (3-8)

$n(T)$  indicates the refractive index at temperature  $T$  [K] and  $p$  the pressure [mbar]. Therefore a change of the atmospheric pressure on the order of a few millibars can cause two-mode beating. A change of the laser gas temperature by about 3°C shows the same effect. The temperature of the laser gas is mainly influenced by the discharge energy. This explains why the PZT has also to be readjusted when the pulse-repetition frequency is changed. Another possible source of refractive-index change is the variation of the laser gas mixture. All this troublesome influences are almost impossible to be controlled in another way than by observing the output pulse and by readjusting the cavity length.

### 3.3.5 Performance

For given ratios  $V/L$  of the circuit, dielectric sheet material and thickness, sheet-to-electrode gap and gas pressure, the gas composition greatly influences the laser performance. Under these circumstances the best gas mixture can be found only experimentally. The relatively close position of our preionizer to the Ernst electrodes

permits optimized laser performance with a mixture relatively rich in CO<sub>2</sub> (cf. Table 3-1 p. 22). An excellent glow discharge without streamers is observed. The pulse-to-pulse energy stability is better than 5 % at a pulse repetition rate of 0.5 Hz and better than 10 % at a repetition rate of 2 Hz. The gas consumption is relatively low since the dielectric corona preionization produces considerably less gas dissociation than other techniques. Nevertheless, higher pulse repetition rates require a faster gas flow. The discharge stability is probably limited by gas density variations due to turbulences. The best discharge stability is empirically found for a gas mixture ratio CO<sub>2</sub> : N<sub>2</sub> : He of about 32 : 7 : 61. Increasing the amount of N<sub>2</sub> in the gas mixture results in a pulse energy up to 40 % or higher. However, the peak power in the gain-switched spike remains constant, since the additional energy is contained in the long tail following the spike. For the production of short pulses the high peak power is essential, not the total pulse energy. Therefore, a high initial spike and a low tail is desired. As pointed out in section 3.3.3 nitrogen, in contrast to carbon dioxide, emits UV radiation in a spectral range suited for the preionization of the laser gas. Thus it is to be expected that omitting the nitrogen in the gas mixture suppresses the long tail in the laser pulse, and also prevents preionization. This is observed experimentally. An amount of nitrogen below the optimum results in a lower pulse energy as well as in a larger pulse-to-pulse fluctuation due to discharge instabilities. Further reduction of the nitrogen content results in insufficient preionization. In this case, the glow discharge constricts to an arc incapable to excite the laser gas. In Table 3-1 (p. 22) the characteristic data of laser I and laser II are listed for comparison.

## 4 The Plasma Shutter

### 4.1 Principle of Operation

After the first report of a laser-induced gas breakdown by Maker et al. (1964) the interaction of high-intensity laser radiation with gas atoms received considerable attention. Smith (1970) used a Q-switched CO<sub>2</sub> laser to determine the gas-breakdown threshold for 10.6 μm radiation. He found that for intensities as high as 10<sup>9</sup> W/cm<sup>2</sup> no self-breakdown occurred. However, an initial low degree of ionization caused subsequent growth of the breakdown. Yablonovitch (1973) observed strong spectral broadening at the instant of gasbreakdown and a sudden drop in the laser power transmitted through the breakdown plasma. Two mechanisms are generally considered important in explaining the beginning of ionization of a gas: multiple photon absorption process and cascade or collisionally induced ionization. The multiple-photon absorption requires simultaneous absorption of a number of photons of energy sufficient to ionize an atom or molecule. In the mid-infrared the photon energy  $h\nu_{\text{CO}_2} \approx 0.12 \text{ eV}$  of the CO<sub>2</sub> laser is considerably smaller than the ionization energy  $\Phi_{\text{ion}} = 5...25 \text{ eV}$  of a gas atom or molecule. This implies that e. g. in nitrogen, where the ionization energy  $\Phi_{\text{N}_2} = 15.6 \text{ eV}$ , more than 130 photons have to be absorbed by a single molecule in an interaction time of approximately 30 fs. The probability of this process depends on the intensity of the laser radiation and the density of the gas. From detailed calculations Smith (1970) states that the intensity required to completely ionize the gas by the multi-photon process is at least an order-of-magnitude larger than the experimentally determined intensity. Also the probability for a multiphoton-ionization process is too small in the infrared to explain complete ionization of a gas, a multiphoton process may ionize the first few molecules and thus initiate the breakdown process. The complete ionization, however, is the result of the cascade-ionization process, which absorbs laser radiation by free electrons colliding with atoms, molecules and ions. An electron from an ionized molecule absorbs energy from the radiation field by the inverse bremsstrahlung process until it has sufficient energy to ionize another molecule upon collision. The result is another free electron. This process continues with an exponential growth rate of the ionization. The statistics of the gas breakdown are therefore mainly influenced by time and locus of the appearance of the first free electrons. These first electrons have to be generated by some direct process, since the electron density in air is less than 10<sup>3</sup> cm<sup>-3</sup> [Tozer, 1965]. Cosmic radiation contributes about 10 free electrons



per  $\text{cm}^3$ . Therefore the probability to find a free electron in a focal volume of  $10^{-8} \text{ cm}^3$  during a 100 ns laser pulse is less than  $10^{-12}$ . Another direct ionization process which is more likely in the infrared than multi-photon ionization is the ionization in the field of a strong electromagnetic wave [Brumme, 1977]. In a classical model it is assumed that a bound electron is accelerated by the first half wave of the field of the incident radiation and is decelerated in the subsequent half wave, so that the average energy gain is zero. However, if the field suffices to accelerate an electron during the first half wave to reach the ionization energy, the molecule is ionized and a free electron is produced to start the cascade-ionization process. Other possible sources of initial electrons are thermoionically emitted electrons from aerosol particles and photoionization of low-ionization impurity atoms [Bekefi, 1976].

Once the gas breakdown has started, the ionized region becomes strongly absorbing and the gas is therefore rapidly heated. This causes fast spherical expansion of the plasma. In the channel of the incident light the plasma forms an absorption wave [Raizer, 1965], called laser-supported absorption wave (LSAW), which grows in the direction towards the laser. The plasma-front propagation speed depends on the laser intensity and the plasma propagation mechanism. It can be as fast as  $2 \cdot 10^6 \text{ m/s}$  [Kwok, 1985]. The incident laser therefore passes a region of locally and temporally rapidly changing refractive index  $n(x,t)$  [Landau and Lifschitz, 1983]

$$n(x,t) = (1 - N(x,t) / N_c)^{1/2}$$

$$\text{with } N_c = \frac{m_e \omega_0^2}{4\pi e^2} \text{ and } \Omega_p = \left( \frac{4\pi N_e e^2}{m_e} \right)^{1/2} \quad (4-1)$$

Here  $N(x,t)$  indicates the electron density in the plasma.  $N_c$  is the critical density where the plasma frequency  $\Omega_p$  reaches the laser circular frequency  $\omega_0$ .  $N_e$  and  $m_e$  denote the electron density and the mass of an electron. As long as  $N(x,t) < N_c$  the refractive index of the gas is close to unity. Hence the beam is transmitted. When the critical density is reached, the refractive index becomes complex. The imaginary part indicates strong absorption of the laser radiation. The fast growth of the plasma is responsible for a fast truncation of the incident beam.

Empirically, we have found the fastest truncation of the incident laser pulse, when the plasma growth starts slightly behind the focus. We assume that this fact is due to geometry of the beam in the focal volume. The plasma starts slightly behind the beam waist and expands rapidly towards the laser, where the beam diameter is smaller and the plasma expands over the entire focal volume. This implies that the plasma growth

should always be initiated at the same point. In order to fulfil this condition and to select the time when the pulse is truncated, a seed plasma produced by an external mechanism is required. This implies that measures must be taken to prevent a self-breakdown. Since the self-breakdown threshold depends on the pressure in the gas, the operating pressure can be adapted for given beam parameters and laser power to prevent self-breakdown. The breakdown threshold for CO<sub>2</sub> laser radiation is a minimum for gas pressures of several atmospheres [Brumme, 1977]. For higher as well as for lower pressures the threshold intensity decreases. In a plasma shutter the operating pressure is consequently kept just below the self-breakdown threshold.

## 4.2 Design of the Plasma Shutter

We designed and tested two plasma shutters. Both consist of an anodized aluminium cell. The cell is sealed and can be evacuated. The optical system of the plasma shutter is a 1:1 Keplerian telescope formed by two identical lenses. The internal focus of the telescope is located in the centre of the cell. The entire plasma shutter is carried by a gimbal mount. This arrangement, together with two translation stages, permits precise positioning of the telescope in the optical axis of the laser. The laser beam enters the cell by one of the lenses, is thus focused to a diffraction limited spot and subsequently recollimated by the second lens before leaving the cell. All surfaces of the lenses are anti-reflection (AR) coated. The first and the last surface of the lenses act as windows and are therefore sealed by indium wire in the lens mounts. The lens mounts are sealed by O-Rings and are screwed into a precision threaded rotation mount, which permits exact focusing of the two lenses even under vacuum. The lens can easily be replaced by another lens with different focal length to investigate the effect of the focal length on the plasma growth. The focal volume is flushed with a clean gas, e. g. nitrogen. The gas pressure is adjustable from vacuum to atmospheric pressure by means of a vacuum pump and a needle valve. Typical operating pressures are 30 to 300 mbar. The aim of the adjustable pressure is to prevent self-breakdown of the laser beam in the focus. Therefore, the gas pressure is chosen to be slightly below self-breakdown of the laser and depends on the gas, the impurities in the gas and the intensity of the laser in the focus. The intensity in the focus is determined by the laser power as well as by the beam parameters and the focusing lens. A collimated Gaussian beam focused by a lens of focal length  $f$  and a clear diameter  $D$  produces a focal spot diameter  $d_0$  [Siegman, 1986]

$$d_o \approx \frac{2f\lambda}{D} \quad (4-2)$$

This result is based on the criterion that the clear aperture  $D$  of the lens is chosen such that 99% of the incident energy is transmitted. By rule of thumb this is the case for a Gaussian beam entering the lens of

$$d(f) \approx \frac{2}{3} D \quad (4-3)$$

diameter. The ratio  $f/D$  is an important measure for accomplishing strong focusing and is called  $f^\#$ , *f-number*, relative aperture, or speed of the lens. However, the critical dimension is the lens diameter as well as the Gaussian beam diameter, which should fill the focusing lens aperture to minimize the focal spot size. A laser with power  $P$  generates a peak intensity  $I_o$  at the centre of the focal spot given by

$$I_o \approx \frac{P}{2(f^\# \lambda)^2} \quad (4-4)$$

Calculations show that ZnSe meniscus lenses with a  $f^\# > 2$  exhibit almost diffraction-limited performance. However for  $f^\# < 2$  less than two a more complex multielement lens is required to correct the spherical aberration. In our shutters we applied single element ZnSe meniscus lenses with 2.5 inch focal length and 1 inch clear apertures (i. e.  $f^\# = 2.5$ ) as well as ZnSe doublets with 1 inch focal length and 1 inch clear diameter (i. e.  $f^\# = 1$ ). The second lens yields a focal spot diameter of approximately  $35 \mu\text{m}$  and intensities up to  $900 \text{ MW/cm}^2$ . So far the two shutters are identical. Yet, they differ in the scheme of triggering the gas breakdown, as described in the following two sections.

#### 4.3 Targets for Optical Triggering

Focusing a laser beam sufficiently intense to produce an optical self-breakdown plasma in air or in a clean gas at atmospheric pressure yields the simplest plasma shutter possible. The occurrence of the breakdown is influenced within certain limits by the gas flux in the focal volume and the pulse repetition rate of the laser. However, no

precise control is possible and the breakdown occurs before the laser pulse reaches its peak power [Mücke 1988; Prettl, 1989].

An improved yet still simple scheme to control the gas breakdown in the plasma shutter is to adjust the pressure in the shutter in such a way that the laser pulse produces a self-breakdown near its peak. Unfortunately, the reproducibility from shot to shot remains poor. This results in significant intensity fluctuation of the generated short pulse. Also this can be tolerated for certain applications, it is not suited for the pulse width determination by second harmonic generation (SHG), where the detected signal is proportional to the square of the pulse intensity.

Kwok and Yablonovitch (1977 b) introduced an optical triggering spark near the focus. A clean gas prevented self-breakdown of the laser. A small portion of the beam is deflected and delayed and then focused on a target located near the focus of the main beam. Thus a surface plasma is generated on the target. This plasma initiates the breakdown of the main beam. We have designed an arrangement [Kälin et al., 1990 a] where the beam is focused into a sealed cell which can be evacuated. This permits to adapt the pressure in the shutter to the power of the applied laser. The pressure is adjusted to lie just below the self-breakdown threshold.

It is well known that the optical gas breakdown on the surface of a solid target requires energy densities up to two orders of magnitudes lower than for a breakdown in air [Thomas, 1975; Kovalev et al., 1979; Bondarenko et al., 1980; Danilychev et al., 1980; Kovalev and Popov, 1981]. This is due to the evaporation of the solid surface [Vilenskaya and Nemchinov, 1969; Bergel'son et al., 1974; Bessarab et al., 1978; Danilychev et al., 1980]. The threshold energy  $E_{thr}$  varies linearly with the absorption coefficient  $\alpha$  of the target [Konov et al., 1983]. However at high intensities, i. e. above  $0.6 \text{ GW/cm}^2$ , a gas breakdown can occur without surface evaporation. This occurs because the incident radiation interferes with reflected radiation from the target surface and thus causes locally intensities near the surface sufficient for a gasbreakdown [Walters et al., 1978]. The surface texture is another important factor. In our plasma shutter we restricted the energy densities on the target as far as possible. We tested and compared various targets for their ability to produce a surface plasma at intensities below  $50 \text{ MW/cm}^2$ . The targets tested were for the first time various metallized graphites besides pure graphite and pure metals, which were used in other laboratories [Kwok and Yablonovitch, 1977 b]. The experimental arrangement as well as detailed results are described elsewhere [Kälin et al. 1990 b]. Here we summarize the main results.

We found on one hand that pure graphite is not suited for our application, since it ceased to produce a surface plasma after a few thousands of laser shots. The failure is mainly due to a rapid surface "burn-out", which shifts the target out of the focus. On

the other hand all the tested metals still formed a surface plasma after 250'000 shots onto the same spot if the energy density in the focus was sufficient (Fig. 4-1). For practical reasons we stopped the measurements after 250'000 shots. In agreement with

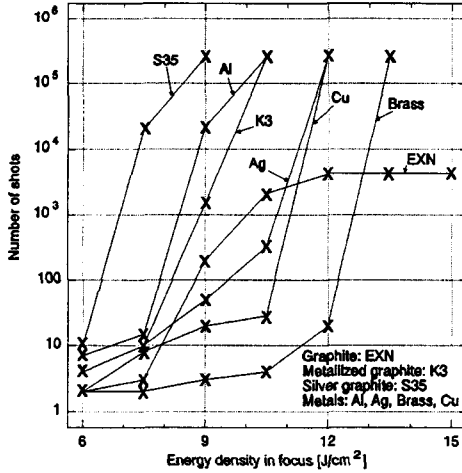


Fig. 4-1: Maximum numbers of pulses with surface-plasma formation at the same spot of various targets vs. energy density in the focus. Note that for all tested targets the measurements were terminated for practical reasons even when they still formed a surface plasma after 250'000 shots.

Kwok and Yablonoitch (1977 b) we found that aluminium forms a surface plasma at the lowest energy density of all tested metals. Subsequently we introduced metallized graphites, designed for use in electric motors and tacho generators. Whilst the behaviour of most of the metallized graphites was comparable to aluminium, silver graphite S35 showed a clearly better performance than all other targets tested. We found no correlation between the suitability of a target and the material properties such as density, resistivity and Cu-content. We attribute the fact that silver graphite differs from pure silver to the content of impurities of graphite and other unknown components. Furthermore the locally heated surface is assumed to undergo chemical reactions with the ambient air. These impurities form microscopic surface defects, which are thermally insulated from the metal. This causes easy evaporation and ionization of microscopic particles [Walters et al., 1978; Kovalev et al., 1979; Weyl et al., 1980; Ursu et al., 1983]. In an earlier experiment Graf and Kneubühl (1983) measured the amount of ejected material per pulse from a metal target. They found that the amount of ejected

metal decreased with increasing ambient gas pressure due to screening of the target surface from the laser radiation by the plasma formed in front of the target.

Also the optical triggering by means of a target close to the focus is relatively easy to achieve and represents a considerable improvement with respect to the self-triggered breakdown, it shows some disadvantages. Changing the operating pressure in the shutter changes the conditions for the forming of a surface plasma and thus requires readjustment. In addition, the target should be located as close as possible to the focus of the main beam, however without obstructing the beam. An increasing distance between target and focal volume results in an intolerable jitter of the truncation time.

#### 4.4 Electrical Triggering by a Laser Triggered Spark Gap

In order to improve the optical triggering and to reduce annoying alignment we investigated a second scheme. Kwok and Yablonovitch (1975 a) have demonstrated that an electrical surface spark instead of a laser-produced surface plasma is also capable of triggering the optical gas breakdown. Again the distance between the surface plasma and the focal volume must be kept below 1 mm in order to minimize the triggering jitter. Hasselbeck et al. (1983) used a needle-resistor spark gap to produce a surface plasma. The advantage of this scheme is that it works with voltages as low as 500 V. However, we found that the surface of the cleaved carbon resistor deteriorates after a few thousand shots and consequently the needle has to be readjusted. Thus, we decided to apply an electric arc discharge directly through the focal volume rather than a surface discharge outside the focal volume. This, however, has the disadvantage to require higher voltages on the order of a few kilovolts, depending on the electrode gap and the pressure in the shutter. In addition, an ultrafast high-voltage switch is required to apply the high-voltage pulse. The jitter of the laser pulse versus the TEA laser trigger pulse is on the order of 200 ns depending on the spark gap used. Therefore, this jitter is larger than the time between the start of the laser pulse and its peak, where we wish to truncate the pulse. Thus, the reference pulse which triggers the discharge in the TEA laser is not suited to trigger the optical breakdown in the plasma shutter. Instead the start of the laser pulse has to be detected to derive a trigger signal for the plasmashutter. For a typical laser pulse duration of 70 ns FWHM the time from the beginning of the pulse to the peak is also approximately 70 ns. A circuit is required capable to detect the pulse and to apply a high-voltage pulse within this relatively short time in the plasma

shutter. The detected signal of the laser pulse is in the millivolt range. It has to be amplified by a fast amplifier to a level suited to trigger a high-voltage pulse generator. Unfortunately, an amplifier shows also a delay between input and output. Therefore the high-voltage pulse generator needs a small delay and a fast rise time. A thyatron circuit is not suited for this application, since it has a typical anode delay time of 100 to 200 ns. A krytron, i. e. a cold cathode switch tube, is capable to switch up to 8 kV. Special fast designs exhibit a delay of 40 ns and a jitter of 5 ns. However, they need a minimum trigger voltage as high as 750V. Pulse generators incorporating thyristors as switches are too slow, while those incorporating avalanche transistors cannot hold the high voltage required.

Therefore, none of the above circuits is capable to produce a high-voltage pulse preceding the peak of the laser pulse. A more promising technique makes use of a laser triggered spark gap (LTSG). Pendleton and Guenther (1965) investigated a ruby-laser-triggered sphere-sphere spark gap. They focused a high-power laser beam within the gas in the spark gap in a way that the beam traversed the gap without impinging on the electrodes. A volume charge along the laser beam produced a localized field distortion and, therefore, a local overvoltage condition to initialize the breakdown. The required switching threshold was several megawatts. The gap conduction was established through electron avalanche and streamer formation. Pulse rise times  $t_r$  and delays  $\Delta t_d$  were typically tens of nanoseconds. Lower trigger thresholds and shorter pulse rise times were achieved by the use of narrow gaps in vacuum, triggered by focusing the laser beam onto the surface of one electrode [Steinmetz, 1968]. In this case the triggering mechanism depends on local heating and thermoionic emission at the irradiated electrode. Pressurized spark gaps are easier to handle and capable to switch voltages up to several megavolts. Also early work on LTSG was devoted to low-jitter switching of high voltages without direct electrical contact and to multiple spark gap synchronization, LTSG's were soon applied for the generation of precisely timed pulse generators [Trevelyan, 1969]. Such pulses are of special interest for fast switching of Pockels and Kerr cells synchronous with the initiating laser pulse in order to select single pulses from a train of mode-locked pulses [Von der Linde et al., 1970]. Nurmikko (1971) constructed a spark gap triggered by a TEA CO<sub>2</sub> laser with a pulse energy of 0.1J and 0.5 MW peak power. He measured an energy threshold approximately a factor of two higher than for a ruby laser. At 10 atmospheres gap pressure the threshold energy was 2 mJ.

We designed and tested a coaxial LTSG (Fig. 4-2 p. 44) of construction similar to that designed for Nd:glass or ruby lasers [Alcock et al., 1970]. The polished brass electrodes have a gap of 1mm. A 1.5 inch focal length ZnSe lens focuses about 1% of the laser

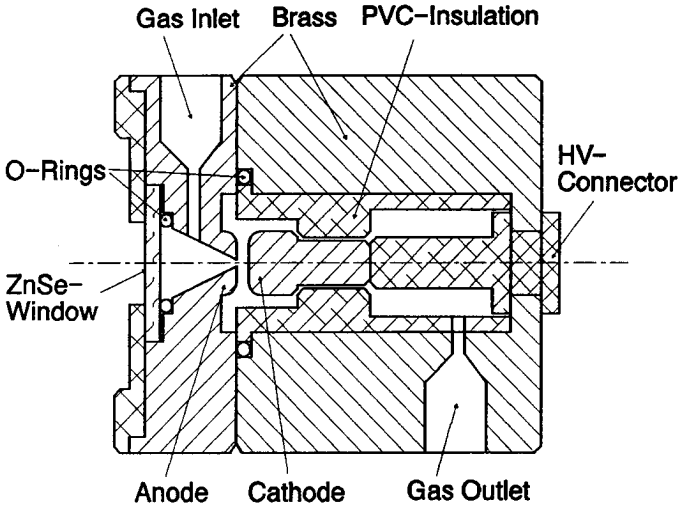


Fig. 4-2: Cross-section of the laser-triggered spark gap.

beam through an anti-reflection coated ZnSe window and a 1.5mm diameter hole in the anode towards the cathode. The lens is located outside the LTSG and thus permits precise focusing. Experiments indicate that delay and jitter are minimum when the focus is about 1 to 2mm behind the target electrode. This is probably due to reflection of the beam on the polished cathode. The reflected beam interferes with the incident and increases locally the intensity of the beam in the gap. The working pressure of 2 to 3 bar of nitrogen permits an operating voltage up to 15 kV. In order to keep the losses of the laser power a minimum, the power directed to the LTSG is derived from a ZnSe flat, which is antireflection (AR) coated on both sides for an incidence angle of  $45^\circ$  and a wavelength of  $10\ \mu\text{m}$ . This ZnSe flat acts as a beam combiner, which aligns the transmitted CO<sub>2</sub> laser beam with a visible pilot beam incident in right angle to the CO<sub>2</sub> laser. The residual reflection of the AR coatings is on the order of 1-2 % and suffices to safely trigger the LTSG. The beamcombiner is located behind the plasma shutter. Thus the laser pulse incident on the cathode is a truncated pulse. This minimizes electrode wear due to the laser impact. The electrode erosion due to electric sparking is also small, since the electric energy loading is modest, i. e. less than 10 mJ at 5 kV.

The LTSG is connected via a coaxial cable (cf. Fig. 1-1, p. 5) with a simple pulse-forming network, which applies a high-voltage pulse with a rise time  $t_r$  of less than 2 ns to two plasma triggering electrodes in the plasmashutter. Actually, the measured rise time was



limited by the response of the high-voltage probe used. These electrodes lie in a plane perpendicular to the optical axis. Since the laser-breakdown plasma expands primarily towards the incident laser, the plasma triggering electrodes should be located slightly behind the plane of optimum focus in order to achieve the fastest truncation time possible. The exact timing is performed by the length of the coaxial cables or alternatively by the reduction of the voltage applied to the LTSG. The latter procedure changes the reduced electric field  $E/p$  in the LTSG and increases both delay and jitter [Duley, 1976]. The classical theory of gas breakdown in a spark gap was modified by Bettis and Guenther (1970) to include the effect of laser ionization at one electrode. They found that the time delay  $\Delta t_d$  between the laser impact and the initiation of breakdown is given by

$$\Delta t_d = \frac{\ln n_c - \ln N_o}{\alpha v} + \frac{d - \chi_c}{S}$$

with  $n_c = N_o \exp(\alpha \chi_c)$  (4-5)

The first term represents the time required by the avalanche discharge to travel a critical distance  $\chi_c$ , where the avalanche converts to a streamer.  $n_c$  denotes the critical number of electrons attained after avalanche propagates the critical distance  $\chi_c$ .  $N_o$  is the initial number of electrons present or produced by the laser impact on the cathode. It varies with time, when the delay is less than the duration of the laser pulse. This certainly holds in our application.  $\alpha$  is the Townsend first ionization coefficient and  $v$  is the relatively low avalanche velocity of  $10^3$  to  $10^6$  m/s.  $\alpha/p$  and  $v$  are functions of the reduced electric field  $E/p$ .  $p$  indicates the pressure in Torr. The second term is the time for streamer propagation over the remaining distance  $d - \chi_c$  for an electrode separation  $d$ . This term can often be neglected, since the streamer velocity  $S$  of  $10^6$  to  $10^7$  m/s is much higher than the avalanche velocity. In this case the equation is reduced to [Bettis and Guenther, 1970]

$$\Delta t_d = \frac{K}{p (E/p)^m}$$
(4-6)

if the term  $(\ln n - \ln N_o)$  in (4-5) is assumed to be constant for a certain range of  $E/p$ . The exponent  $m$  is primarily determined by the dependence of  $\alpha/p$  on  $E/p$ , since  $v$  varies slowly with  $E/p$ . Thus, if  $E/p$  is kept constant, the delay  $\Delta t_d$  varies with  $1/p$ . The delay  $\Delta t_d$  can therefore be adjusted by changing the applied voltage and pressure simultaneously, or by changing gap distance and pressure while keeping  $E/p$  constant.

Since in our application a fixed delay is required, a coaxial cable as delay line is the simplest solution. The fine adjustment is then performed by adapting the high voltage applied on the LTSG.

We tested the performance of the LTSG for various pulse energies focused on the cathode versus the percentage of the applied selfbreakdown voltage (SBV) [Kálin et al., 1990 a]. The results are shown in Fig. 4-3.

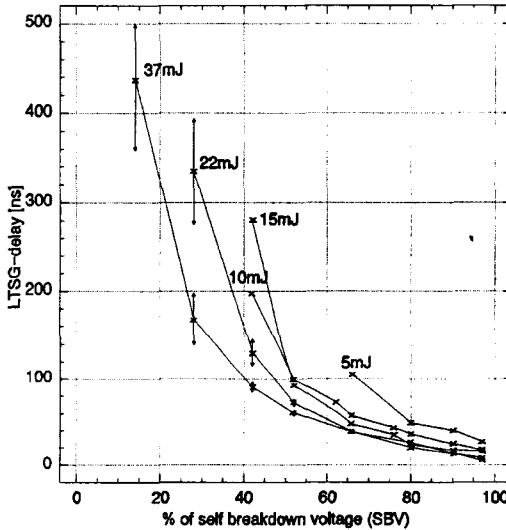


Fig. 4-3: Delay of LTSG firing vs. applied self-breakdown voltage for various pulse energies. The jitter for pulse energies of 22 mJ and 37 mJ is also shown.

As expected from (4-5) the delay decreases with increasing pulse energy, since the number  $N_o$  of initially laser-generated electrons increases also with the pulse energy. Decreasing the voltage from 97% SBV increases the delay  $\Delta t_d$  initially almost linearly. However, below  $\approx 60\%$  SBV the delay and also the jitter increase rapidly. For pulse energies of 37 mJ the LTSG still fires at 14% SBV, whilst for pulse energies of 5 mJ triggering is uncertain for less than 65% SBV. Since in all cases the delay is shorter than the total pulse duration, the effective energy threshold is lower than the pulse energy. For the application of the LTSG in the plasma shutter approximately 10 mJ are appropriate to trigger the LTSG before the pulse reaches its peak. In order to minimize the jitter,  $E/p$  should be chosen to give an operating voltage of 80% SBV or higher.

Under these conditions the jitter is clearly less than 5 ns. Thus, the resulting amplitude fluctuation at the instant of truncation is negligible compared to the pulse stability of the TEA laser from shot to shot. Fig. 4-4 shows a typical pulse truncated in the plasmashutter. Up to now both, LTSG and plasma shutter, exhibit maintenance-free operation for already more than  $10^7$  shots without any observed degradation of performance.

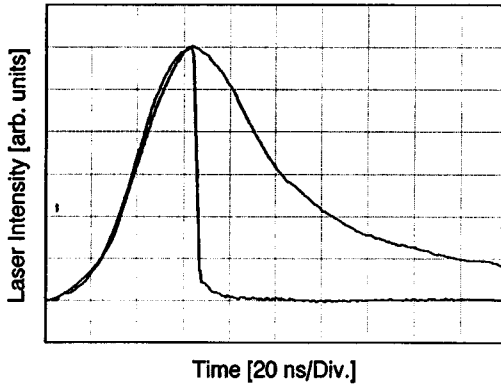


Fig. 4-4: Truncated and untruncated single-mode  $CO_2$ -laser pulses.

## 5 The Hot CO<sub>2</sub>-Cell

### 5.1 Spectral Filters in Short-Pulse Systems

As pointed out in the linear system analysis in section 2.3 short pulses can be produced from a rapidly truncated pulse, if an appropriate spectral filter is found. The task of the spectral filter is to reject the incident laser wavelength while transmitting the sideband frequencies produced by the rapid plasma growth. The rejection ratio has to be sufficient to clearly separate the short OFID pulse from the incident laser pulse. For a simple estimation the energy of the incident laser pulse can be compared with the OFID-pulse energy. The energy of a TEA laser pulse truncated in its maximum and incident into the filter is approximately  $E_{in} = \frac{1}{2} \cdot P_o \cdot \tau_{TEA}$ , where  $P_o$  is the peak power and  $\tau_{TEA}$  is the FWHM pulse duration of the TEA laser pulse. Assuming the same peak power in the OFID-pulse the short pulse energy is  $E_{out} = P_o \cdot \tau_{OFID}$ . Since the ratio  $\tau_{OFID} : \tau_{TEA}$  is on the order of 1 : 1000 the incident laser wavelength must be attenuated by a multiple of this ratio according to the desired signal to background ratio.

### 5.2 Previous Designs

Among the spectral filters mentioned in section 2.1 the resonant-material absorber is the most promising since it offers an excellent signal-to-background rejection ratio at reasonable expense. Yablonovitch and Goldhar (1974) introduced resonantly absorbing CO<sub>2</sub> gas as spectral filter. A 1 m long silica tube contained 30 to 130 mbar of CO<sub>2</sub> and was wrapped with heating tape, insulation and aluminium foil. Heating of the gas is necessary in order to populate the lower laser level and therefore to increase the absorption coefficient. Experimentally it was found that for CO<sub>2</sub> the absorption coefficient is almost constant in the range 400 °C to 900 °C [Kwok, 1978]. The laser beam was passing the cell and was reflected by a mirror to give a 2 m path having a rejection ratio of 10<sup>2</sup>. Kwok and Yablonovitch (1975 b) used a 3.05 m long glass pipe, which was insulated by 10 cm of glass wool and an aluminium foil. The tube was heated to 420 °C by an electric power of 400 W from a Variac. At the operating pressure of 30 to 40 mbar the absorption factor was 2.5 · 10<sup>4</sup> in a double pass through the tube. Kwok (1978) reported two major problems associated with the hot CO<sub>2</sub> cell. The first problem is saturation of absorption by an intense laser beam and probably relates to the laser itself, since high-intensity spikes of a beating laser cause saturation rather than smooth single mode pulses. The result of the saturation is a poor OFID-pulse-to-prepulse ratio.

However, even with reproducible smooth TEA-laser pulses saturation occurs whenever a low CO<sub>2</sub> pressure is chosen in order to produce longer OFID pulses. In order to solve this problem the hot-cell length should be adapted to the operating pressure to guarantee that the absorption is constant for all pressures. Such a construction, however, is difficult to realize, since the cell is heated to 400 °C and should be vacuum tight. An approach may consist of several hot cell segments with various lengths and the combination of the appropriate segments with the aid of mirrors for a given pressure. This, however, requires many windows and mirrors and complicates construction and alignment. Yet, it would provide modest improvement only. Therefore, a compromise between the length of the hot cell and the feasible operating pressure range has to be found. The second problem of the hot cell reported is a vertical beam deflection by the hot gas in the horizontal cell. This is explained by a small amount of thermal gradient in the cell. Kwok (1978) gave an approximative formula for the vertical deflection  $h$  assuming that the temperature gradient is constant and independent of the pressure inside the cell:

$$h = -8\pi N\alpha L^2 \cdot \frac{\nabla T}{T} \quad (5-1)$$

where  $N$  is the density of gas,  $\alpha$  the polarizability,  $L$  the length of the cell and  $\nabla T$  the temperature gradient. Kwok (1978) measured a beam deflection as large as 7 mm downward after a double pass of the 3 m long cell. This represents a serious problem, since the beam deflection depends on the operating pressure. Once the system is aligned with the hot cell evacuated all elements behind the hot cell will be misaligned after filling the hot cell with CO<sub>2</sub>. In order to solve this problem Kwok (1978) measured the deflection for various pressures of air and CO<sub>2</sub>. The deflections of air and CO<sub>2</sub> differ at a given pressure because of the different polarizabilities  $\alpha$ . Consequently, the right amount of air is used during the alignment to compensate the deflection. A more thorough solution of this problem is the minimization of the thermal gradient by a good thermal insulation. The tube must not be put on a table which could act as a heat sink. Instead, the tube is surrounded by air in order to avoid heat diffusing into the table. Furthermore, the optical path of the laser beam in the hot cell can be chosen so that a residual temperature gradient is compensated when the beam passes the cell twice. Thus also the astigmatism resulting from the passage of a slightly converging beam through a medium with a refractive index gradient is minimized.

Another problem is the sealing of the hot-cell windows. Robinson et al. (1988) designed a window assembly using a custom-machined gasket of PTFE (Teflon). Pressurizing

and heating the window assemblies heats the PTFE to its melting point and thereby causes it to flow and effect the seal. Robinson et al. (1988) noted that the shape of the PTFE gasket is crucial to its success. Overheating of the PTFE must be avoided to prevent the release of highly toxic decomposition products. This technique is difficult to be applied for Brewster windows of rectangular shape. In order to minimize losses by reflection, windows mounted in Brewsters angle are required. Antireflection (AR) coated windows cannot be applied since the AR coating will not withstand the temperature of 400 °C. In a previous design Robinson et al. (1983) sealed a BaF<sub>2</sub> window by means of a high-temperature silicone-rubber adhesive. Also the sealant was rated by the manufacturer at 260 °C for continuous operation and for 315 °C for short periods, they found that the sealant could withstand several cycles up to 350 °C. However, no effective seal could be made with NaCl windows, probably due to the high solubility of NaCl. On the other hand, NaCl windows are suitable candidates as their melting point is 801 °C and in addition they are inexpensive. The rated safest operating temperature is 400 °C. In effecting a vacuum seal it should be noticed that NaCl is hygroscopic. Therefore, the windows have to be replaced from time to time. Keeping the temperature of the windows slightly higher than the ambient air prolongs the life of the NaCl windows considerably. The final hot-cell construction is described in more detail in the following chapter.

### 5.3 Present Design

The construction of the hot cell can be explained with the aid of Fig. 5-1. The cell consists of a Pyrex<sup>®</sup> glass tube of 85mm outer and 77 mm inner diameter. Three tubes

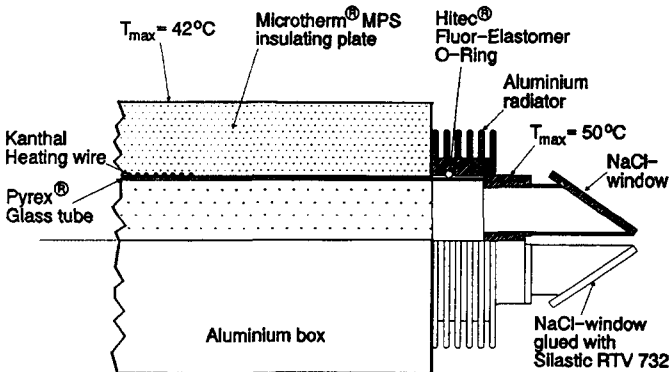


Fig. 5-1: Construction detail of the hot CO<sub>2</sub>-cell.

have been built with a length of 1.5m, 3m and 4m. All have the same diameter and can easily be interchanged. The cell is heated by a 1 mm thick Kanthal heating wire with a resistance of  $1.77 \Omega/m$ . 230 turns with a pitch of 5 mm form a heating coil with approximately  $110 \Omega$  resistance and a heating power of 440 W at 220 V. The 3 m and the 4 m cell are wrapped with 2 respective 3 such heating coils, giving a total heating power of 880 W respective 1300 W. The ends of the tubes are not heated at a length of about 20 cm. The windings are fixed by a high temperature ( $1000^\circ\text{C}$ ) alkalisilicate-based glue in order to prevent short circuit of the windings due to the thermal expansion of the hot wire. The electric current is fed by fiberglass-insulated copper wires. A type K (Chromel vs. Alumel) thermocouple located in the center of each coil measures the surface temperature of the glass tube. An electronic circuit controls the temperature of each coil independently to  $\pm 2^\circ\text{C}$  of the nominal value. A solid-state relay with a zero-voltage-crossing detector switches the electric power of the heating wires on or off when the AC voltage is zero. Therefore, the power delivered to the heating wire is varied by the ratio of the turn on/turn off time of the triac rather than by changing the phase angle during which the triac is conducting. This zero-voltage switching minimizes RFI generated during the load current turn-on. The nominal value of the temperature can be set between room temperature and  $400^\circ\text{C}$ . Also the heating power is sufficient to achieve higher temperatures, there is no need to exceed  $400^\circ\text{C}$  since there is no significant increase of the absorption coefficient of CO<sub>2</sub> at higher temperatures. Temperatures higher than  $900^\circ\text{C}$  also populate the upper laser level and the absorption decreases. Temperatures above  $450^\circ\text{C}$  would permanently deform the evacuated glass tube and should therefore be avoided.

As pointed out in section 5.2 the tube has to be carefully thermally insulated to minimize a vertical temperature gradient resulting in a refractive index gradient and, consequently, a vertical beam deflection. For this reason the tube is embedded in a box bent from a 0.8 mm thick aluminium sheet. The cover is fixed by screws. The quadratic cross section of the box has an outer dimension of 210 mm. The length is 140 mm shorter than the glass tube so that the ends of the glass tube show through the insulation box. Inside the box the walls are insulated by Microtherm<sup>®</sup> MPS heat insulating plates of 4 cm thickness. This material manufactured by Micropore International Limited has a relatively low thermal conductivity, especially at high temperatures. For  $400^\circ\text{C}$  on the hot end its thermal conductivity is  $0.026 \text{ Wm}^{-1}\text{K}^{-1}$  compared to  $0.06 \text{ Wm}^{-1}\text{K}^{-1}$  for conventional insulating material. The remaining hollow space between the tube and the insulating box is filled with glass wool. When the tube is heated to  $400^\circ\text{C}$ , the maximum outside temperature of the aluminium box is  $42^\circ\text{C}$ . The warm-up time is

approximately 90 minutes. When the nominal value is reached less than 50% of the nominal electric power suffices to maintain the temperature.

At the two ends the glass tube is closed by an aluminium termination carrying two NaCl windows arranged in Brewsters angle. The clear aperture is 30 mm. The necessary vacuum seal is obtained by a Hitec<sup>®</sup> Fluor-Elastomer O-ring rated at 200 °C for permanent use. In order to avoid temperatures higher than 200 °C the aluminium termination has no thermal insulation. Instead the surface is enlarged to form a radiator. Since the glass tube is not heated at a length of 20 cm at the ends and the thermal conductivity of glass is relatively low the aluminium temperature remains below 35 °C when the cell is evacuated. However, when the cell is filled with hot gas the heat transport is mainly by the gas and the temperature rises to 50 °C at a pressure of 600 mbar. The NaCl windows are also sealed by the same type of O-Ring. Alternatively, the windows can be glued with Silastic 732 RTV. In both cases an excellent vacuum seal is achieved. In order to ensure stability of the optical alignment, one of the aluminium terminators is fixed on the table. The second is mounted on a rail aligned in with the optical axis. It can glide axially. This is necessary to compensate the thermal expansion of the glass tube which can reach 5 mm for a tube of 4 m length. The laser beam enters the hot cell through the lower window on the side with the fixed windows and leaves the cell on the opposite side. Two adjustable mirrors mounted on the table deflect the laser beam each by 90 degrees back to the upper window of the hot cell. In this case the beam passes the hot gas upside-down. Assuming a constant vertical thermal gradient in the cell this construction effects a compensation of beam deflection and astigmatism by the double pass of the beam. In fact, the downward deflection of a He-Ne-Laser beam observed 3 m after a double pass in the hot cell has a maximum of about 1 mm at 400 mbar and decreases to zero at 600 mbar and at pressures below 400 mbar. This demonstrates that the residual thermal gradient is not exactly linear as assumed. However, the remaining deflection is small and is of no importance for most experiments.



## 6 OFID-Pulse Characteristics

### 6.1 Theoretical Pulse Shapes

The linear system analysis in section 2.3 permits the calculation of the OFID-pulses obtained under a number of various operating conditions. The output electric field  $E_{out}(t)$  is obtained by the inverse Fourier transform of eq. (2-6). For other switching functions than Heaviside's unit step function (2-4) the output field  $E_{out}(t)$  can not be calculated analytically. Instead a numerical solution computed on a PC by application of the fast Fourier transform algorithm (FFT) [Brigham, 1974] provides the required results. The calculation is necessary for an estimation of the influence of various parameters on the expected OFID-pulse shape. Fig. 6-1 (p. 54) is a plot of the calculated temporal intensity profiles for various truncation functions for the plasma shutter. The truncation functions are listed in Table 6-1.

Plasmashutter Truncation Function	Fig.	Relative Amplitude	OFID-FWHM $\Delta t$ [ps]	Autocorrel. FWHM $\Delta \tau$ [ps]	$\Delta t / \Delta \tau$
Instantaneous	6-1 A	1.11	44.1	76.5	0.58
$I(t) = I_o(1-t/\tau_f)$ $\tau_f = \tau_{pl}$	6-1 B	1.03	44.6	78.4	0.57
$E(t) = E_o(1-t/\tau_f)$ $\tau_f = 1.58 \cdot \tau_{pl}$	6-1 C	0.95	48.1	81.4	0.59
$E(t) = \frac{E_o}{2}[1 - \tanh(t/\tau_f)]$ $\tau_f = 0.54 \cdot \tau_{pl}$	6-1 D	0.88	53.1	80.4	0.66
$E(t) = E_o \exp[-(t/\tau_f)^2]$ $\tau_f = 1.19 \cdot \tau_{pl}$	6-1 E	0.84	55.5	83.0	0.67
$E(t) = E_o \exp[-(t/\tau_f)]$ $\tau_f = 0.91 \cdot \tau_{pl}$	6-1 F	0.73	66.6	90.4	0.74

Table 6-1: Calculated OFID-pulse characteristics for various truncation functions

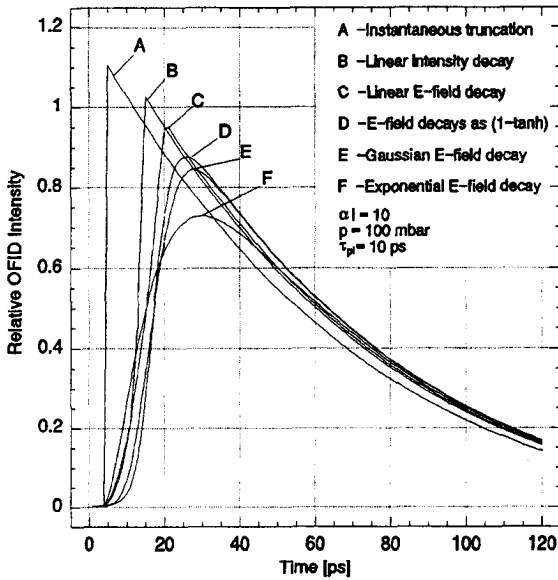


Fig. 6-1: Calculated OFID-pulse shapes for various truncation functions.

$\tau_{pl}$  is defined as the time the plasma needs to reduce the transmitted intensity from 90% to 10%.  $\tau_f$  is the corresponding time for the electric field. The ratio  $\tau_f / \tau_{pl}$  is of the order of unity. The exact value depends on the truncation function and is also given in Table 6-1 (p. 53). In the same table the OFID-pulse duration  $\Delta t$  full width at half maximum (FWHM) is also shown, together with the autocorrelation half width  $\Delta \tau$ . The ratio  $\Delta t / \Delta \tau$  depends on the exact pulse shape. The amplitude of the OFID pulse is computed relative to the incident amplitude. The OFID pulses show an asymmetry in their temporal profile. Whilst the pulse tail decays exponentially in all cases as expected for free induction decay, the leading edge and therefore the amplitude, pulse shape and pulse duration strongly depend on the truncation function assumed.

The most important parameter, however, is not the truncation function itself, but the truncation time  $\tau_{pl}$ . As shown in Fig. 6-2 and Table 6-2 the relative intensity diminishes with increasing  $\tau_{pl}$  whilst the pulse duration increases.

Truncation Time $\tau_{pl}$ [ps]	Relative Amplitude	OFID-FWHM $\Delta t$ [ps]	Autocorrel. FWHM $\Delta \tau$ [ps]	$\Delta t / \Delta \tau$
1	1.08	45.1	77.0	0.59
10	0.88	53.1	80.9	0.66
20	0.72	60.0	83.0	0.72
30	0.61	66.2	84.2	0.79
40	0.51	72.1	80.4	0.90

Table 6-2: Calculated OFID-pulse characteristics for various truncation times  $\tau_{pl}$

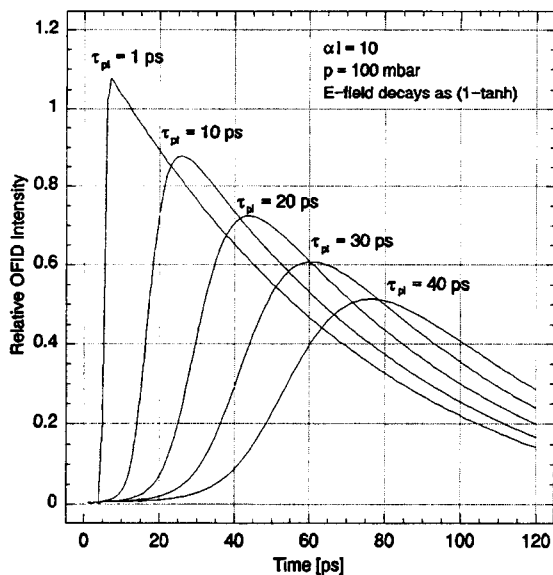


Fig. 6-2: Variation of the OFID-pulse shape with the truncation time  $\tau_{pl}$ .

The shortest pulses which can be generated by this technique are determined by the truncation speed of the plasma shutter. For a given truncation speed the pulse duration can be varied by changing the pressure in the hot CO<sub>2</sub> absorber cell. Unfortunately, the intensity will also vary as shown in Fig. 6-3 and Table 6-3.

Hot CO <sub>2</sub> cell pressure [mbar]	Relative Amplitude	OFID-FWHM $\Delta t$ [ps]	Autocorrel. FWHM $\Delta \tau$ [ps]	$\Delta t / \Delta \tau$
100	0.88	53.1	80.9	0.66
200	0.71	30.1	47.0	0.64
300	0.55	21.8	32.9	0.66
400	0.45	17.6	26.2	0.67
500	0.38	15.2	22.6	0.67
600	0.32	13.5	20.3	0.67
700	0.27	12.3	18.6	0.66

Table 6-3: Calculated OFID-pulse characteristics for various pressures in the hot CO<sub>2</sub> cell

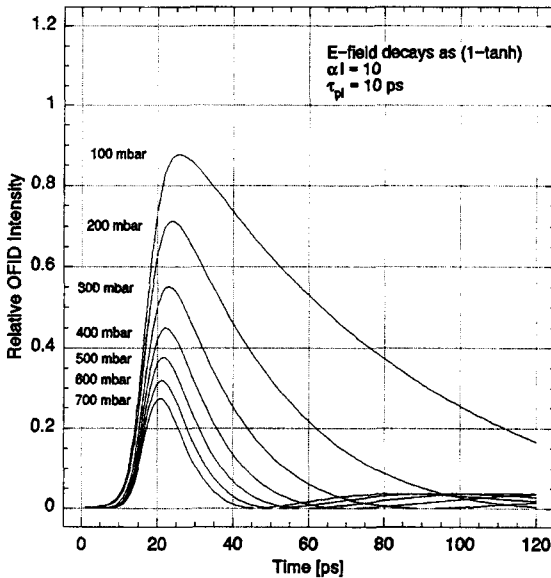


Fig. 6-3: Calculated OFID-pulse shape for various pressures in the hot CO<sub>2</sub> cell.

Another parameter influencing pulse shape and duration is the length of the hot cell. An optimum could be achieved by adapting the length of the hot CO<sub>2</sub> cell to the operating pressure. This is difficult to achieve as mentioned in section 5.2. Therefore, the length of the cell is fixed to give a sufficient pulse-to-background ratio.

The influence of the asymmetric spectrum of an exponentially growing plasma as measured by Yablonovitch (1974 b) was also calculated. We found, that the theoretical pulse duration is slightly increasing with the asymmetry. However, the increase is less than 10% for a up to 10 times blue-shifted spectrum.

## 6.2 Direct Pulse Measurements

The measurement of the temporal profile as well as the duration of 10  $\mu\text{m}$  laser pulses shorter than  $\approx 1\text{ns}$  cannot be performed directly. This is due to both the limited rise time of the infrared detectors available and the limited bandwidth of the oscilloscope. Instead, an indirect technique with subpicosecond time resolution as described in section 6.3 is required. Nevertheless, it is useful to combine a fast infrared detector with a fast transient recorder in order to directly observe whether an OFID pulse is generated or not. Furthermore, the saturation in a too short hot CO<sub>2</sub> cell resulting in a pretail preceding the OFID pulse can be observed. Among the fastest detectors sensitive at a wavelength of 10  $\mu\text{m}$  are the pyroelectric detector model P5-00 of Molelectron Inc. (USA) and the photon drag detector model PDM-2 of Edinburgh Instruments (GB). The pyroelectric detector has an order of magnitude higher sensitivity than the photon drag detector. The sensitive area, however, is only  $1\text{mm}^2$  in order to minimize the detector capacitance. Thus, when the detector is terminated by a 50 Ohm coaxial line and a 50 Ohm amplifier the typical detector rise time is  $t_{rd} \approx 110\text{ ps}$ . Our Tektronix 7912HB transient digitizer with the 7A29P input amplifier has a specified rise time  $t_r \leq 575\text{ ps}$  and can be approximated as a low-pass filter. The expected total detector/scope rise time is therefore  $t_{rt} \leq 600\text{ps}$ . The measured rise time is  $t_{rm} \approx 450\text{ ps}$ . This is not sufficient to resolve temporally the measured OFID pulse. Instead, for pulses with a rise time  $t_{rp} < t_{rt}$  the detection system is integrating the short pulse and, therefore, the peak of the measured signal is proportional to the pulse energy. Assuming a constant peak power of the short pulses generated at different pressures in the hot CO<sub>2</sub> cell, the measurement of the pulse energies permits a fast and simple estimation of the dependence of pulse duration on the pressure in the hot CO<sub>2</sub> cell. The results are shown in Fig. 6-4 (p. 58). The pulse characteristics of our OFID-laser systems are compared in Table 6-4 (p. 58).

	Laser System I	Laser System II
Single-mode-pulse energy	0.3 J	1.0 J
Pulse duration (FWHM)	100 ns	70 ns
Peak power	$\approx 1.3$ MW	$\approx 7$ MW
OFID pulse energy (33 ps)	$\approx 15$ $\mu$ J	$\approx 90$ $\mu$ J
OFID peak power (33 ps)	$\approx 0.5$ MW	$\approx 3$ MW

Table 6-4: Pulse characteristics of our OFID-laser systems

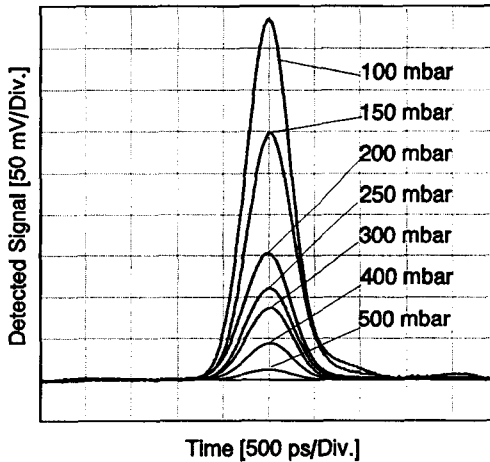


Fig. 6-4: OFID-pulses measured with bandwidth-limited detector/scope system for various pressures of the hot  $\text{CO}_2$  gas in the spectral filter.

### 6.3 Autocorrelation Pulse Measurements

Since it is obviously not possible to determine the duration of the OFID pulses by a direct measurement, another technique has to be applied. Many auxiliary techniques have been developed in high-speed physics which permit to examine fast signals, e. g. the streak technique and the sampling technique. The mechanical streak technique with a rotating mirror arrangement has a resolution of the order of 1 ns whilst the electron-optical streak camera offers a resolution of the order of 1 ps, but is limited to

the visible and near-infrared spectral range [Herrmann and Wilhelm, 1987]. A method successfully used for many decades, particularly in electronics, is the correlation method. The signal  $I(t)$  convoluted with itself yields the second-order autocorrelation function  $G^{(2)}(\tau)$ , whilst the convolution of  $I(t)$  with a subsidiary signal gives the cross-correlation function. A special case of the cross-correlation function is the sampling technique. This method, however, requires a fast detector and a fast multiplier. A method capable to provide the required resolution is the optical autocorrelation, where the multiplication is performed by optical means. The very first measurements of picosecond duration optical pulses were performed using the optical autocorrelation technique by second-harmonic generation (SHG) [Weber, 1967]. Since we applied this method to measure the duration of the OFID pulses, we will briefly explain the principle. The optical pulse is divided in a Michelson interferometer into two beams, each with an intensity  $I(t)$ . These beams travel different paths before they are recombined and focused into a nonlinear crystal. The temporal overlap of the two pulses at the crystal can be varied by mechanically changing one of the path lengths. The amount of SHG signal detected is a maximum when the two pulses are coincident and decreases as one is delayed a time  $\tau$  with respect to the other. Depending on the arrangement and the crystal it is possible that no SHG signal is generated when either beam is blocked or when the two beams arrive at sufficiently different times. Weber (1967) proposed and later demonstrated [Weber, 1968] an arrangement, where two orthogonally polarized pulses pass collinearly through a nonlinear KDP crystal. The crystal is orientated such that phase-matched SHG is produced only when both polarizations are present, i. e. when the two pulses temporally overlap. Maier et al. (1966) and Armstrong (1967) demonstrated somewhat different techniques also giving background-free SHG signal. The normalized second-order autocorrelation function of the intensity  $I(t)$  is

$$G^{(2)}(\tau) = \frac{\langle I(t) \cdot I(t + \tau) \rangle}{\langle I^2(t) \rangle} \quad (6-1)$$

The brackets indicate an average over a sufficiently long time interval. If  $I(t)$  is a single isolated pulse,  $G^{(2)}(\tau)$  vanishes for sufficiently large delay  $\tau$  and its half-width  $\Delta\tau$  provides a measure of the duration of  $I(t)$ . The problem of measuring the pulse duration  $\Delta t$  is thus reduced to the measurement of the mirror displacement. This mechanical problem can be solved with the required accuracy, e. g. 1 ps corresponds to a mirror displacement of 0.15 mm. The actual ratio  $\Delta\tau/\Delta t$  of the autocorrelation-halfwidth versus the pulse-halfwidth depends on the precise pulse shape. However, the uncer-

tainty in this estimate is less than a factor of two. For example if the theoretical pulse shape is assumed to be Gaussian, then the ratio becomes  $\Delta\tau/\Delta t = \sqrt{2}$ . Nevertheless, since (6-1) is obviously symmetric, regardless of any asymmetry in  $I(t)$  as expected for OFID pulses,  $G^{(2)}(\tau)$  is not suited to determine the pulse shape. Precise determination of the pulsewidth requires an assumption about the temporal shape of  $I(t)$ . In order to determine  $I(t)$  uniquely, higher-order correlation functions are required. It has been demonstrated that the exact knowledge of  $G^{(2)}(\tau)$  and  $G^{(3)}(\tau)$  is sufficient to describe all higher orders of  $G^{(k)}(\tau)$ ,  $k > 2$ , and hence the temporal shape  $I(t)$  of the pulse itself [Ippen and Shank, 1977].

In our autocorrelator we applied a collinear arrangement and the same polarization in both beams. Therefore, the measured autocorrelation signal is not background-free, i. e. there is always a SHG signal detected, even when the two beams do not temporally overlap. This has the advantage that proper contrast provides assurance that the central peak of the autocorrelation function is resolved [Ippen and Shank, 1977]. The SHG signal  $S(t)$  is in this case given by

$$S(\tau) = 2S_0 [1 + 2G^{(2)}(\tau) + r(\tau)] \quad (6-2)$$

$S_0$  is the SHG signal measured with one partial beam blocked.  $r(\tau)$  is a rapidly varying fringe-like component due to interferences of the two partial beams. It averages to zero over several optical periods and is generally not observed experimentally. The so-called contrast ratio  $K$  is

$$K = S(0) / S(\infty) \quad (6-3)$$

The contrast is  $K = 3$  for pulses of limited duration. It would be only  $K = 1.5$  for bandwidth-limited noise [Herrmann and Wilhelmi, 1987]. Therefore, by simply determining the contrast ratio it is possible to test whether the central peak of the autocorrelation function has been properly resolved. This is a great advantage over the background-free method. The disadvantage is the interference term, especially at low pulse repetition frequencies, where only a limited number of mirror positions are scanned in order to restrict the measurement duration.

Our autocorrelator consists of a Ge plate AR-coated on one surface and acting as beamsplitter on the other. Each of the two partial beams is reflected back by a mirror to the beamsplitter, which recombines the two beams in a direction orthogonal to the incident beam. Subsequently, the two parallel beams are focused by a lens into a nonlinear crystal. In this context we introduced for the first time polycrystalline ZnSe



and GaAs samples for the SHG [Kesselring et al. 1990]. One of the two mirrors can be translated along the beam by a digitally controllable stepper-motor. A successful measurement requires careful beam alignment. In order to eliminate the SHG signal generated in the ZnSe lenses of the plasma shutter and thermal radiation of the plasma itself a filter is required between the focusing lens and the SHG crystal. Another filter between the crystal and the SHG detector blocks the fundamental frequency. The detector is a liquid nitrogen cooled InSb detector. A matched low-noise preamplifier amplifies the second-harmonic signal before it is fed into a digital storage oscilloscope (DSO) LeCroy 9450. The DSO is connected with an Olivetti personal computer (PC) via the general purpose interface bus (GPIB). The PC repeatedly accumulates the correlation signal like a multi-channel analyzer and controls the mirror displacements by means of a stepper-motor. Fig. 6-5 shows a typical measured multishot autocorrelation curve. Since the curve seems quite noisy at the first moment, it needs some explanation.

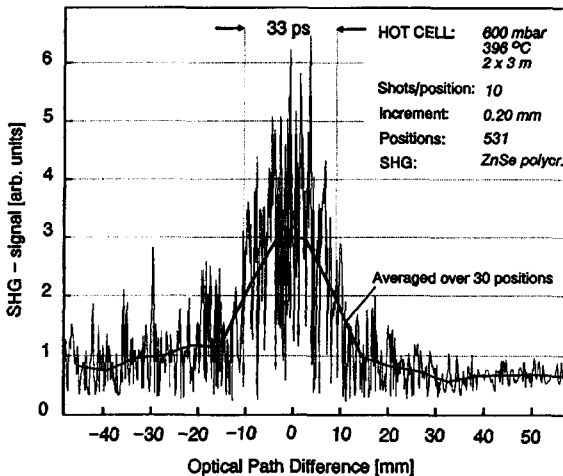


Fig. 6-5: Multishot autocorrelation plot measured at 531 discrete mirror positions and subsequently averaged over 30 positions to suppress the interferences.

The curve was scanned point by point. The SHG signal of 10 subsequent laser pulses has been averaged at each mirror position. A total of 531 positions were scanned, yielding 5310 pulses for the entire autocorrelation curve. This corresponds to a meas-

urement duration of approximately  $1\frac{1}{2}$  hour. The long-term stability of the system is mainly influenced by the single longitudinal mode stability of the laser, since both, plasmashutter and hot cell, operate maintenance free. The shot-to-shot power stability of the TEA-laser of  $\pm 5\%$  produces a fluctuation in the SHG signal of about  $\pm 10\%$ . However, when mode-beating is present, the intensity at the instant of truncation can be more than twice as high as for a smooth pulse or can be much smaller, depending on the instant of truncation. Whilst the intensity of the OFID pulse is proportional to the intensity at the instant of truncation, the SHG signal is proportional to the square of the intensity and is tremendously fluctuating in this case.

For these reasons such a pulse-duration measurement requiring many subsequent shots over a long period is difficult. For comparison, mode-locked short-pulse lasers have pulse-repetition frequencies of the order of several ten megahertz and therefore provide a much better statistic in a fraction of a second. Another reason for the fluctuation of the SHG signal is the interference term  $r(\tau)$  in (6-2). When the collinear autocorrelator is perfectly aligned, the interferences can be easily observed by fine tuning the mirror position by means of a PZT translator. Measuring only in those positions where constructive interferences are observed increases the contrast to  $K = 8$  [Alcock and Corkum, 1980]. In contrary, when measuring only in those positions showing destructive interferences the autocorrelation signal decreases from unity if the pulses do not overlap temporally to zero if they overlap exactly. In general, the mirror is randomly positioned, regardless of interferences. Therefore, the measured SHG signal is somewhere in between the two extreme positions and partial interferences are observed. This fact contributes the largest amount to the fluctuation of the signal measured in Fig. 6-5 (p. 61).

When measuring over many positions and integrating the signal in a boxcar averager as usual, the interference effects are averaged and no longer observed. In our experiment the data are digitally stored for each mirror position. Therefore, the interferences are not averaged. However, when the data are averaged over a sufficient number of randomly selected subsequent positions the interferences are averaged. The smooth curve in Fig. 6-5 (p. 61) shows the result for an average of the data over 30 subsequent positions. In this case the contrast is approximately  $K = 3$  as expected from (6-2) and (6-3). This confirms that the peak of the autocorrelation curve has been resolved.

#### 6.4 Multiple Breakdown Phenomena

From the lens selection discussion in section 4.2 it is clear that a 2.5 inch focal length lens yields about six times smaller intensities in the focus than a one inch focal length lens. The diameter of the focus is increased and also the depth of focus. From this the main difference one expects is that the plasma needs more time to expand over the beam diameter and therefore the truncation speed is slower. In fact we observed several subsequent breakdowns within less than 1 ns to several 10 ns, depending on the gas and the gas pressure. Such a multiple breakdown blocks the transmission for a short time and becomes transparent and rapidly blocks again as shown in Fig. 6-6A. The gas in the plasma shutter was helium at a pressure of 40 mbar. When such a truncated pulse passes the spectral filter several OFID pulses result as demonstrated in Fig. 6-6B.

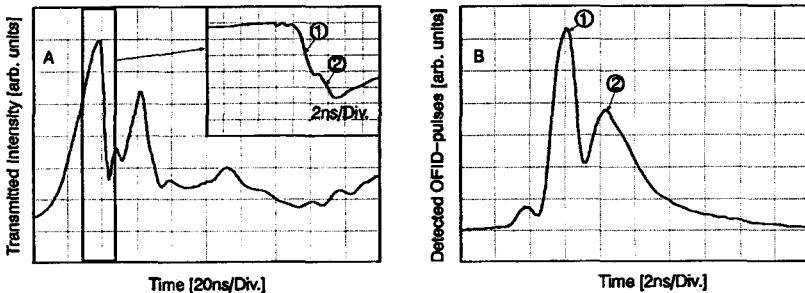


**Fig. 6-6:** Multiple breakdowns: Trace A shows the  $\text{CO}_2$ -laser intensity transmitted through the plasma generated in helium at a pressure of 40 mbar. The focal length of the lens was 2.5 inches. Note that under these conditions no self-breakdown occurs. The breakdown was initiated by the LTSG-discharge. The inserted curve is a tenfold expansion of the truncation edge. It demonstrates, that there are at least two subsequent breakdowns at an interval of approximately 2 ns. The detector/scope system is not capable to resolve temporally the fast transients. Trace B is the detected OFID signal for a pressure of 100 mbar of hot  $\text{CO}_2$ . This trace is also not resolved by the system. Nevertheless, the peaks and the asymmetry indicate that more than three subsequent OFID pulses are generated.

The plasma shutter pressure dependence is demonstrated in Fig. 6-7. The OFID-pulse train shows wider intervals at 100 mbar helium. With helium in the plasma shutter the energy of the OFID pulses is higher at pressures below 50 mbar, indicating a faster truncation than at higher pressures. The time between the subsequent pulses is too short to be resolved by the detector/scope system. Nevertheless, the presence of more than a single pulse can be seen from the asymmetric pulse shape. Above 100 mbar the pulses are separated by approximately 15 ns.

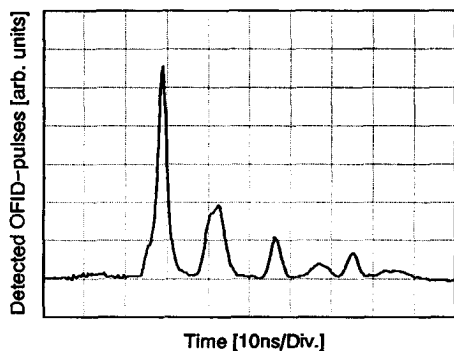


**Fig. 6-7:** Detected pulse train of OFID pulses. Increasing the helium pressure in the plasma shutter to 100 mbar expands the OFID-pulse train. The pressure in the hot CO<sub>2</sub> gas is also 100 mbar. Again the pulses are not resolved by the detector/scope system. Nevertheless, one observes more than seven pulses of various energies.

Similar results, yet with different intervals between the pulses are obtained for nitrogen and argon in the plasma shutter. When the beam is focused by a lens of one inch focal length multiple OFID pulses can be observed with helium in the plasma shutter. However, nitrogen and air show no such effects. Thus the geometry of the focal volume, the gas, the gas pressure and the laser intensity determine the transmission of the plasma shutter. We attribute the multiple-OFID pulses to self-focusing effects in the gas, which cause several high-intensity spots in the relatively large focal volume and therefore the plasma grows from several points at different times, each blocking off a portion of the beam. For some operating pressures plasma oscillations were also observed.

Beside self-focusing, lens aberration effects are well known to produce several spots with increased intensity in the focal volume [Evans and Grey Morgan, 1969]. Self-focusing effects produced by a ruby laser in air were observed and investigated by Bakos et al. (1981). They interpreted these effects by nonuniform heating of the plasma and by the ponderomotive force of light. Also for the full understanding of the phenomena observed in the CO<sub>2</sub> laser-generated plasma further investigations are necessary, the multiple short pulses can be attributed to OFID in the hot CO<sub>2</sub> gas and probably under certain conditions to multiple photon echos [Shoemaker, 1978].

## 7 Conclusion

The combination of a plasma shutter with a saturable absorber in an OFID system is a reliable method to generate CO<sub>2</sub> laser pulses as short as 30 ps with a peak power of several Megawatts. The main advantage of this technique compared to mode-locking is the generation of single short pulses with an excellent signal-to-background ratio. The limit for the shortest pulse duration by this arrangement seems to be 30 ps. It is mainly determined by the finite speed of the plasma shutter. Important points for reliable operation of an OFID system are single-mode TEA-laser pulses as well as an suitable method to trigger the absorbing plasma.

The introduction of a laser-triggered spark gap which initiates a high-voltage discharge across the focal volume permits a stable and fast truncation of the TEA-laser pulse. Adjusting the pressure in the plasma shutter extends the useful operating conditions to a wide range of laser power. The hot CO<sub>2</sub> absorber cell is a comparatively simple and cheap spectral filter offering an excellent suppression of the incident long CO<sub>2</sub> laser pulse. A disadvantage of this pulse-shaping technique is certainly the efficiency of less than 0.1%. For many experiments an energy threshold is required rather than a power threshold. In those cases the energy of the OFID pulses may be too low. However, when the spectral filter is reduced in length, the OFID pulse is preceded by a pretail due to saturation in the absorber. In this case the high peak power is still contained in the short OFID pulse, also the total energy is increased considerably. This arrangement has the advantage that after the OFID pulse no pedestal remains which affects the experiment. When the spectral filter is omitted a sharply truncated TEA-laser pulse results. Such a pulse contains about a quarter of the energy of a the typically long-tailed TEA-CO<sub>2</sub> laser pulse, yet it is a well terminated. This permits the observation of the post-pulse development of the experiment. Such pulses have a great potential of applications e. g. for the optical pumping of FIR lasers, for detector tests and for material characterization by photo-acoustically induced surface displacements.

## 8 References

- R. L. Abrams (1974)  
"Broadening coefficients for the P(20) CO<sub>2</sub> laser transition"  
*Appl. Phys. Lett.* **25**, 609-611
- A. J. Alcock and P. B. Corkum (1980)  
"Ultra-short pulse generation with CO<sub>2</sub> lasers"  
*Phil. Trans R. Soc. Lond.* **A298**, 365-376
- A. J. Alcock and A. C. Walker (1974)  
"Generation and detection of 150-psec mode-locked pulses from a multi-atmosphere CO<sub>2</sub> laser"  
*Appl. Phys. Lett.* **25**, 299-301
- A. J. Alcock, M. C. Richardson, and K. Leopold (1970)  
"A Simple Laser-Triggered Spark Gap with Subnanosecond Risetime"  
*Rev. Sci. Instrum.* **41**, 1028-1029
- A. J. Alcock, P. B. Corkum, and D. J. James (1975)  
"A fast scalable switching technique for high-power CO<sub>2</sub> laser radiation"  
*Appl. Phys. Lett.* **27**, 680-682
- L. Allen and J. H. Eberly (1975)  
*Interscience Monographs and Texts in Physics and Astronomy*  
Volume XXVIII: "Optical Resonance and Two-level Atoms"  
John Wiley & Sons, New York
- J. A. Armstrong (1967)  
"Measurement fo Picosecond Laser Pulse Widths"  
*Appl. Phys. Lett.* **10**, 16-18
- R. V. Babcock, I. Liberman and W. D. Partlow (1976)  
"Volume Ultraviolet Preionization from Bare Sparks"  
*IEEE J. Quantum El.* **QE-12**, 29-34

J. S. Bakos, I. B. Földes and Zsuzsa Sörlei (1981)

"High-intensity narrow light pulse produced by self-focusing in laser spark"

J. Appl. Phys. **52**, 627-634

N. G. Basov, E. M. Belenov, V. A. Danilychev and A. F. Suchkov (1971)

"High-Pressure Pulsed CO<sub>2</sub> Laser"

Sov. Journ. of Quantum El. **3**, 306-307

A. J. Beaulieu (1970)

"Transversely Excited Atmospheric Pressure CO<sub>2</sub> Lasers"

Appl. Phys. Lett. **16**, 504-505

G. Bekefi ed. (1976)

"Principles of Laser Plasmas"

John Wiley & Sons, New York

V. I. Bergel'son, A. P. Golub', I. V. Nemchinov and S. P. Popov (1974)

"Formation of a plasma in a vapor layer produced by the action of laser radiation on a solid"

Sov. J. Quantum El. **3**(4), 288-292

A. V. Bessarab, V. M. Romanov, V. A. Samylin and A. I. Funtikov (1978)

"Shielding time of a surface irradiated by a CO<sub>2</sub>-laser"

Sov. Phys. Tech. Phys. **23**(8), 995-996

J. R. Bettis and A. H. Guenther (1970)

"Subnanosecond-Jitter Laser-Triggered Switching at Moderate Repetition Rates"

IEEE J. Quantum El. **QE-6**, 483-491

R. E. Beverly (1978)

"Light Emission from High-Current Surface-Spark Discharges"

Chapter VI, Progress in Optics **16**, ed. E. Wolf, North Holland, Amsterdam

R. E. Beverly, R. H. Barnes, C. E. Moeller and M. C. Wong (1977)

"Ultraviolet spectral efficiencies of surface-spark discharges with emphasis on the iodine photodissociation laser pumpband"

Appl. Opt. **16**, 1572-1577

F. Bloch (1946)

"Nuclear Induction"

Phys. Rev. **70**, 460-474

F. Bloch, W. W. Hansen and M. Packard (1946)

"The Nuclear Induction Experiment"

Phys. Rev. **70**, 474-485

A. V. Bondarenko, V. S. Golubev, E. V. Dan'shchikov, F. V. Lebedev,

A. F. Nastoyashchii and A. V. Ryazanov (1980)

"Thermal ionization breakdown of the air near the surfaces of metals irradiated by a CO<sub>2</sub> laser"

Sov. Phys. Dokl. **25** (8), 616-618

R. Bracewell (1965)

"The Fourier Transform and Its Applications"

McGraw-Hill Book Company, New York

R. G. Brewer and R. L. Shoemaker (1972)

"Optical Free Induction Decay"

Phys. Rev. A **6**, 2001-2007

E. O. Brigham (1974)

"The Fast Fourier Transform"

Prentice-Hall

G. Brumme (1977)

"Laserinduzierter Gasdurchbruch"

Ph. D. Thesis, TH Darmstadt

D. E. Caddes, L. M. Osterink and R. Targ (1968)

"Mode locking of the CO<sub>2</sub> laser"

Appl. Phys. Lett. **12**, 74-76



T. Y. Chang (1973)

"Improved Uniform-Field Electrode Profiles for TEA Laser and High-Voltage Applications"

Rev. Sci. Instr. **44**, 405-407

R. A. Chodzko, H. Mirels, F. S. Roehrs and R. J. Pedersen (1973)

"Application of a Single-Frequency Unstable Cavity to a CW HF Laser"

IEEE J. Quantum El. **QE-9**, 523-530

P. B. Corkum, A. J. Alcock, D. F. Rollin and H. D. Morrison (1978)

"High-power subnanosecond pulses from an injection modelocked multiatmosphere CO<sub>2</sub> oscillator"

Appl. Phys. Lett. **32**, 27-29

V. A. Danilychev, V. D. Zvorykin, I. V. Kholin and A. Yu. Chugunov (1980)

"Investigation of the dynamics of plasma formation near a target acted on by microsecond CO<sub>2</sub> laser pulses"

Sov. J. Quantum El. **10** (12), 1518-1521

W. W. Duley, (1976)

In "CO<sub>2</sub> Lasers, Effects and Applications"

Academic Press, New York

R. Dumanchin and J. Rocca-Serra (1969)

"Augmentation de l'énergie et de la puissance fournie par unité de volume dans un laser à CO<sub>2</sub> en régime pulsé"

C. R. Acad. Sc. Paris **269**, 916-917

H. Egger, M. Dufour and W. Seelig (1976)

"Inhomogeneities in TEA laser discharges"

J. Appl. Phys. **47**, 4929-4933

G. J. Ernst (1977)

"Single-frequency, atmospheric pressure CO<sub>2</sub> laser"

Rev. Sci. Instr. **48**, 1281-1283

G. J. Ernst (1982)

"A 10 cm Aperture, High Quality TEA CO<sub>2</sub> Laser"

Opt. Comm. **44**, 125-129

G. J. Ernst (1984)

"Uniform-Field Electrodes with Minimum Width"

Opt. Comm. **49**, 275-277

G. J. Ernst and A. G. Boer (1978)

"Construction and Performance Characteristics of a Rapid Discharge TEA CO<sub>2</sub> Laser"

Opt. Comm. **27**, 105-110

L. R. Evans and C. Grey Morgan (1969)

"Lens Aberration Effects in Optical-Frequency Breakdown of Gases"

Phys. Rev. Lett. **22**, 1099-1102

B. J. Feldman and J. F. Figueira (1974)

"Generation of subnanosecond CO<sub>2</sub> laser pulses at 10.6  $\mu$ m by pulse compression techniques"

Appl. Phys. Lett. **25**, 301-303

C. A. Fenstermacher, M. J. Nutter, M. J. Rink and K. Boyer (1971)

"Electron Beam Initiation of Large Volume Electrical Discharges in CO<sub>2</sub> Laser Media"

Bull. Am. Phys. Soc. **16**, 42

R. P. Feynman, F. L. Vernon and R. W. Hellwarth (1957)

"Geometrical Representation of the Schrödinger Equation for Solving Maser Problems"

J. Appl. Phys. **28**, 49-52

R. P. Feynman R. B. Leighton and H. Sands (1964)

"The Feynman Lectures on Physics"

Addison-Wesley, Reading, Massachusetts

J. F. Figueira and H. D. Sutphin (1974)

"Generation of multiband 1-ns pulses in CO<sub>2</sub> lasers"

Appl. Phys. Lett. **25**, 661-663

R. L. Fork, C. H. Brito Cruz, P. C. Becker, C. V. Shank (1987)

"Compression of optical pulses to six femtoseconds by using cubic phase compensation"

Opt. Lett. **12**, 483

R. Fortin, M. Gravel and R. Tremblay (1971)

"Helical TEA-CO<sub>2</sub> Lasers"

Can. J. Phys. **49**, 1783-1793

A. F. Gibson, M. F. Kimmit, and C. A. Rosito (1971)

"Passive Mode Locking of a High-Pressure CO<sub>2</sub> Laser with a CO<sub>2</sub> Saturable Absorber"

Appl. Phys. Lett. **18**, 546-548

A. Girard (1974)

"The Effects of the Insertion of a CW, Low-Pressure CO<sub>2</sub> Laser into a TEA CO<sub>2</sub> Laser Cavity"

Opt. Comm. **11**, 346-351

A. Gondhalekar and E. Holzhauser (1973)

"Single Longitudinal Mode Operation of High Pressure Pulsed CO<sub>2</sub> Lasers"

Phys. Lett. **46A**, 229-230

H. P. Graf and F. K. Kneubühl (1983)

"Temporal and Spatial Evolution of the Laser-Induced Plasma in Methane"

Appl. Phys. **B 31**, 53-61

D. E. Gray coordinating ed. (1972)

"American Institute of Physics Handbook"

Third edition, Mc Graw Hill, New York

E. L. Hahn (1950)

"Nuclear Induction Due to Free Larmor Precession"

Phys. Rev. 77, 297-298

M. Hasselbeck, L. Huang, S. C. Hsu, and H. S. Kwok (1983)

"High-speed, low-cost laser-triggered plasma shutter"

Rev. Sci Instrum. 54, 1131-1134

V. Hasson and H. M. von Bergmann (1976)

"High pressure glow discharges for nanosecond excitation of gas lasers and low inductance switching applications"

J. Phys. E9, 73-76

V. Hasson and H. M. von Bergmann (1980)

"Spatial control of pulsed high-pressure pre-ionisation stabilised glow discharges"

J. Phys. E: Sci. Instrum. 13, 632-638

J. Herrmann and B. Wilhelmi (1987)

"Lasers for Ultrashort Light Pulses"

Akademie-Verlag, Berlin

E. P. Ippen and C. V. Shank (1977)

"Techniques for Measurement"

in "Ultrashort Light Pulses" Ed. S. L. Shapiro

Springer-Verlag, Berlin

S. A. Jamison and A. V. Nurmikko (1978)

"Generation of picosecond pulses of variable duration at  $10.6 \mu\text{m}$ "

Appl. Phys. Lett. 33, 598-600

T. W. Johns and J. A. Nation (1972)

"Ionization Instability in Atmospheric-Pressure Gas Discharges"

Appl. Phys. Lett. 20, 495-496

A. W. Kälin and P. J. Vonesch (1983)

"Stickstofflaser zur Auslösung von Elektronenschwärmen"

Diploma Thesis, ETH Zurich

A. W. Kälin, R. Kesselring, J. Boogman, H. Cao, H. J. Schötzau and F. K. Kneubühl (1990 a)

"Improved Plasma Shutter for OFID 50 ps 10  $\mu\text{m}$  CO<sub>2</sub> Lasers"

Int. J. of Infrared & Millimeter Waves 11 (1), 49-54

A. W. Kälin, R. Kesselring, H. J. Schötzau and F. K. Kneubühl (1990 b)

"New Plasma Shutters for Picosecond-Pulse Optical-Free-Induction-Decay 10  $\mu\text{m}$  CO<sub>2</sub> Lasers"

Proc. Int. Conf. "Lasers 90", SOQUE, San Diego, Dec. 1990, 115-118

W. Kaiser, ed. (1988)

"Ultrashort Laser Pulses and Applications"

Springer-Verlag, Berlin, Topics in Applied Physics Vol. 60

R. Kesselring, R. Castagnetti, A. W. Kälin and F. K. Kneubühl (1990)

"Second Harmonic Generation with 30 ps OFID and 100 ns TEA 10  $\mu\text{m}$  CO<sub>2</sub> Laser Pulses in Polycrystalline Nonlinear Materials"

Proc. Int. Conf. "Lasers 90", SOQUE, San Diego, Dec. 1990, 119-125

F. K. Kneubühl and M. W. Sigrist (1991)

In "Laser" 3rd ed.

Teubner, Stuttgart

V. I. Konov, Yu. V. Lavrent'ev, Yu. I. Stepanov, N. I. Chapliev

and A. V. Shirkov (1983)

"Dependence of the threshold of formation of an air breakdown plasma near copper mirrors on the absorption coefficient of their surface at the wavelength of 10.6  $\mu\text{m}$ "

Sov. J. Quantum El. 13(8), 1128-1130

A. S. Kovalev and A. M. Popov (1981)

"Gas breakdown by a CO<sub>2</sub> laser beam near a metal surface without rapid evaporation"

Sov. Phys. Tech. Phys. 26 (1) 39-41

- A. S. Kovalev, A. M. Popov and A. T. Rakhimov (1979)  
"On the mechanism of breakdown of gases by the emission from a CO<sub>2</sub> laser near a metal surface"  
Sov. Phys. Colloq. **49** (C7), 759-760
- H. S. Kwok (1978)  
"Picosecond CO<sub>2</sub> Laser Pulses and Intramolecular Energy Relaxation in SF<sub>6</sub>"  
Ph. D. dissertation, Harvard University, Cambridge MA
- H. S. Kwok (1985)  
"Picosecond CO<sub>2</sub> Laser Pulses and their Applications"  
Infrared Phys. **25**, 53-59
- H. S. Kwok and Eli Yablonovitch (1975 a)  
"Electrical triggering of an optical breakdown plasma with subnanosecond jitter"  
Appl. Phys. Lett. **27**, 583-585
- H. S. Kwok and E. Yablonovitch (1975 b)  
"CO<sub>2</sub> oscillator-pulse shaper-amplifier system producing 0.1 J in a 500 ps laser pulse"  
Rev. Sci. Instr. **46**, 814-816
- H. S. Kwok and Eli Yablonovitch (1977 a)  
"30-ps CO<sub>2</sub> laser pulses generated by optical free induction decay"  
Appl. Phys. Lett. **30**, 158-160
- H. S. Kwok and Eli Yablonovitch (1977 b)  
"A simple self-triggered plasma shutter"  
Opt. Comm. **21**, 252-254
- J.-L. Lachambre, P. Lavigne, G. Otis and M. Noël (1976)  
"Injection Locking and Mode Selection in TEA-CO<sub>2</sub> Laser Oscillators"  
IEEE J. Quantum El. **QE-12**, 756-764
- A. K. Laflamme (1970)  
"Double Discharge Excitation for Atmospheric Pressure CO<sub>2</sub> Lasers"  
Rev. Sci. Instr. **41**, 1578-1581

- H. M. Lambertson and P. R. Pearson (1971)  
"Improved Excitation Techniques for Atmospheric Pressure CO<sub>2</sub> Lasers"  
Electron. Lett. **7**, 141-142
- L. D. Landau and E. M. Lifschitz (1983)  
"Lehrbuch der theoretischen Physik", Band X: "Physikalische Kinetik"  
Akademie Verlag, Berlin
- K. A. Laurie and M. M. Hale (1971)  
"A Pin-Electrode Atmospheric-Pressure CO<sub>2</sub> Laser"  
IEEE J. Quantum El. **QE-7**, 530-531
- D. A. Leonard (1965)  
"Saturation of the Molecular Nitrogen Second Positive Laser Transition"  
Appl. Phys. Lett. **7**, 4-6
- D. A. Leonard (1967)  
"The 5401-Å Pulsed Neon Laser"  
IEEE J. Quantum El. **QE-3**, 133-135
- J. J. Lowke, A. V. Phelps and B. W. Irwin (1973)  
"Predicted electron transport coefficients and operating characteristics  
of CO<sub>2</sub>-N<sub>2</sub>-He laser mixtures"  
J. Appl. Phys. **44**, 4664-4671
- M. Maier, W. Kaiser and J. A. Giordmaine (1966)  
"Intense Light Bursts in the Stimulated Raman Effect"  
Phys. Rev. Lett. **17**, 1275-1277
- P. D. Maker, R. W. Terhune and C. M. Savage (1964)  
"Optical third harmonic generation"  
Proc. 3rd Int. Conf. on Quantum El. Paris, **2**, 1559-1576
- R. Marchetti, E. Penco, and G. Salvetti (1983)  
"Compact Sealed TEA CO<sub>2</sub> Lasers with Corona-Discharge Preionization"  
IEEE J. Quantum El. **QE-19**, 1488-1492

J. H. McCoy (1969)

"Continuous Passive Mode locking of a CO<sub>2</sub> Laser"

Appl. Phys. Lett. **15**, 353-354

R. Mücke (1988)

"Erzeugung kurzer CO<sub>2</sub>-Laserpulse mit Hilfe des Optischen Freien Induktions-Zerfalls

Diploma Thesis, University Regensburg

A. V. Nurmikko (1971)

"A CO<sub>2</sub>-Laser-Triggered Spark Gap"

IEEE J. Quantum El. **QE-7**, 470-471

A. Nurmikko, T. A. DeTemple and S. E. Schwarz (1971)

"Single-Mode Operation and Mode Locking of High-Pressure CO<sub>2</sub> Lasers by Means of Saturable Absorbers"

Appl. Phys. Lett. **18**, 130-132

A. J. Palmer (1974)

"A physical model on the initiation of atmospheric-pressure glow discharges"

Appl. Phys. Lett. **25**, 138-140

Y.-L. Pan, A. F. Bernhardt and J. R. Simpson (1972)

"Construction and Operation of a Double-Discharge TEA-CO<sub>2</sub> Laser"

Rev. Sci. Instr. **43**, 662-666

C. K. N. Patel (1964)

"Continuous-Wave Laser Action on Vibrational-Rotational Transitions of CO<sub>2</sub> "

Phys. Rev. **136**, A1187-A1193

P. R. Pearson and H. M. Lamberton (1972)

"Atmospheric Pressure CO<sub>2</sub> Lasers Giving High Output Energy Per Unit Volume"

IEEE J. Quantum El. **QE-8**, 145-149

W. K. Pendleton and A. H. Guenther (1965)

"Investigation of a Laser Triggered Spark Gap"

Rev. Sci. Instr. **36**, 1546-1550



W. Prettl (1989)

University Regensburg  
Private Communication

I. I. Rabi (1937)

"Space Quantization in a Gyating Magnetic Field"  
Phys. Rev. **51**, 652-654

Yu. P. Raizer (1965)

"Heating of a gas by a powerful light pulse"  
Sov. Phys. JETP **21**(5), 1009-1017

M. C. Richardson, A. J. Alcock, K. Leopold and P. Burtyn (1973)

"A 300-J Multigigawatt CO<sub>2</sub> Laser"  
IEEE J. Quantum El. **QE-9**, 236-243

A. M. Robinson and N. Sutton (1979)

"High temperature absorption in 10.4- $\mu$ m band of CO<sub>2</sub>"  
Appl. Optics **18**, 378-385

A. M. Robinson, P. Haswell, and M. Billing (1983)

"High-temperature, high-pressure 10- $\mu$ m absorption cell"  
Rev. Sci. Instrum. **54**, 117-118

A. M. Robinson, M. Billing, and D. Garand (1988)

"500°C infrared absorption cell"  
Rev. Sci. Instrum. **59**, 249-251

W. Rogowski (1923)

"Die elektrische Festigkeit am Rande des Plattenkondensators"  
Archiv für Elektrotechnik **12**, 1-15

C. Rolland and P. B. Corkum (1986)

"Generation of 130-fsec midinfrared pulses"  
J. Opt. Soc. Am. **B 3**, 1625-1629

A. J. Schwab and F. W. Hollinger (1976)

"Compact High-Power N<sub>2</sub> Laser: Circuit Theory and Design"

IEEE J. Quantum El. QE-12, 183-188

H. Seguin and J. Tulip (1972)

"Photoinitiated and photosustained laser"

Appl. Phys. Lett. 21, 414-415

K. Shimoda (1984)

"Introduction to Laser Physics"

Springer Series in Optical Sciences, Vol. 44.

Springer-Verlag, Berlin

R. L. Shoemaker (1978)

"Coherent Transient Infrared Spectroscopy"

in Steinfeld ed.: "Laser and Coherence Spectroscopy"

Plenum Press, New York

A. E. Siegman (1974)

"Unstable Optical Resonators"

Appl. Optics 13, 353-366

A. E. Siegman (1986)

In "Lasers"

University Science Book, Mill Valley, California

D. C. Smith (1970)

"Gas Breakdown with 10.6- $\mu$ m-Wavelength CO<sub>2</sub> Laser Radiation"

J. Appl. Phys. 41, 4501-4505

L. L. Steinmetz (1968)

"Laser-Triggered Spark Gap"

Rev. Sci. Instr. 39, 904-909

- H. Tashiro, T. Shimada, K. Toyoda and S. Namba (1984)  
"Studies on Injection Locking of a TEA-CO<sub>2</sub> Laser for Stable High-Power Operation"  
IEEE J. Quantum El. QE-20, 159-165
- P. D. Thomas (1975)  
"Laser absorption wave formation"  
AIAA J. 13 (10), 1279-1286
- B. A. Tozer (1965)  
"Theory of the ionization of gases by laser beams"  
Phys. Rev. 137, 6A, 1665-1667
- B. Trevelyan (1969)  
"A Simple Laser-triggered Spark Gap for Kilovolt Pulses of Accurately Variable Timing"  
Opto-Electronics 1, 62-64
- I. Ursu, I. Apostol, D. Barbulescu, V. Lupei, I. N. Mihailescu, A. Popa, A. M. Prokhorov, N. I. Chapliev and V. I. Konov (1983)  
"On the influence of surface condition on air plasma formation near metals irradiated by microsecond TEA-CO<sub>2</sub> laser pulses"  
Proc. SPIE Int. Soc. Opt. Eng. 398, 361-265
- G. G. Vilenskaya and I. V. Nemchinov (1969)  
"Sudden increase in absorption of laser radiation and associated gasdynamic effects"  
Sov. Phys. Dokl. 14(6), 560-563
- D. Von der Linde, O. Bernecker and A. Laubereau (1970)  
"A Fast Electrooptic Shutter for the Selection of Single Picosecond Laser Pulses"  
Opt. Comm. 2, 215-218
- B. Walter (1985)  
"Dielectrics for corona preionisation of a TEA laser"  
J. Phys. E: Sci. Instrum. 18, 279-281

- C. T. Walters, R. H. Barnes and R. E. Beverly III (1978)  
"Initiation of laser-supported detonation (LSD) waves"  
J. Appl. Phys. **49**(5), 2937-2949
- H. P. Weber (1967)  
"Method for Pulsewidth Measurement of Ultrashort Light Pulses Generated by Phase-Locked Lasers using Nonlinear Optics"  
J. Appl. Phys. **38**, 2231-2234
- H. P. Weber (1968)  
"Generation and Measurement of Ultrashort Light Pulses"  
J. Appl. Phys. **39**, 6041-6044
- J. A. Weiss and L. S. Goldberg (1972)  
"Single Longitudinal Mode Operation of a Transversely Excited CO<sub>2</sub> Laser"  
IEEE J. Quantum El. **QE-8**, 757-758
- G. Weyl, A. Pirri and R. Root (1980)  
"Laser ignition of plasma of aluminum surfaces"  
AIAA J. **19**(4), 460-469
- W. J. Witteman (1987)  
In "The CO<sub>2</sub> Laser"  
Springer Series in Optical Sciences, Vol 53.  
Springer-Verlag, Berlin
- O. R. Wood and S. E. Schwarz (1968)  
"Passive Mode Locking of a CO<sub>2</sub> Laser"  
Appl. Phys. Lett. **12**, 263-265
- E. Yablonovitch (1973)  
"Spectral Broadening in the Light Transmitted through a Rapidly Growing Plasma"  
Phys. Rev. Lett. **31**, 877-879
- E. Yablonovitch (1974 a)  
"Self-Phase Modulation of Light in a Laser-Breakdown Plasma"  
Phys. Rev. Lett. **32**, 1101-1104

E. Yablonovitch (1974 b)

"Self-phase modulation and short-pulse generation from laser breakdown plasmas"  
Phys. Rev. **A10**, 1888-1895

E. Yablonovitch (1975)

"Generation of a Short Optical Pulse of Arbitrary Shape and Phase Variation"  
IEEE J. Quantum El. **QE-11**, 789-791

E. Yablonovitch and J. Goldhar (1974)

"Short CO<sub>2</sub> laser pulse generation by optical free induction decay"  
Appl. Phys. Lett. **25**, 580-582

D. Yu. Zaroslov, N. V. Karlov, G. P. Kuz'min and S. M. Nikiforov (1978)

"Spectral characteristics of vacuum ultraviolet preionization sources for CO<sub>2</sub> lasers"  
Sov. J. Quantum El. **8**, 695-700

### Acknowledgement

I am deeply obliged to Prof. Dr. F. K. Kneubühl for allowing me to start this project and for his continual support and encouragement throughout the course of the research. Special thanks I also owe to Prof. Dr. Ing. W. S. Zaengl for reading and commenting on my thesis. I am also very grateful to Prof. W. J. Witteman and Prof. G. J. Ernst, Twente University of Technology, Enschede, NL and Prof. Cui Dafu, Prof. Cao Hongru, Prof. T. L. Kopiczynski, PD Dr. H. J. Schötzau and PD Dr. M. W. Sigrist for their advice and stimulating discussions.

Most people from the Infrared Physics Lab in some way or another helped me with this project. Robert Kesselring was my office mate and started many fruitful disputes. I am also grateful to Albert Wirth, Daniel Bhend, Cornel Andreoli, Andreas Hermann and Xavier Donath and the technical staff of the Physics Department for their technical support. The students Nick Wetter, Andres Thöny, Jan Boogman and Oliver Seipel contributed to measurements and computer software for this project.

Special thanks go to my parents for their generosity. I am also grateful to my wife Marianne for her love and emotional support. She encouraged me to start and to continue the PhD project.

This study was supported by the Swiss National Science Foundation, the GRD of the EMD and the ETH Zürich.

### Curriculum Vitae

I was born in Euthal-Einsiedeln, Switzerland, on May 24, 1958 where I attended primary school. Subsequently I studied at the "Stiftsschule Einsiedeln" in Einsiedeln and finished with a Matura Type A in 1978. In the same year I started to study Electrical Engineering at the Swiss Federal Institute of Technology, ETH Zürich. In spring 1984 I received a Dipl. Ing. (M. S.) degree in Electrical Engineering with a thesis on " Stickstofflaser zur Auslösung von Elektronenschwärmen" in the "Institut für Hochspannungstechnik" by Prof. W. S. Zaengl. During the next two years I worked in industry in the field of electro-optical precision-instruments. In 1986 I joined the Infrared Physics Laboratory of the new Institute of Quantum Electronics at the Swiss Federal Institute of Technology, ETH Zürich, as an assistant working with Prof. F. K. Kneubühl in research on short-pulse CO<sub>2</sub> lasers.